www.DeepakPublishing.com

Heine, T. et al. (2015): JoSS, Vol. 4, No. 2, pp. 329–356
(Peer-reviewed article available at www.jossonline.com)

www. JoSSonline.com

A CubeSat Concept for Multipoint Ionospheric GPS Occultation

Thomas R. P. Heine, Mark B. Moldwin, Shasha Zou, Jessica Arlas, Ambarish Desai, Brandon Heidt, Steve McCarty, Adelina Nastasoiu, and Vritika Singh

Department of Atmospheric, Oceanic and Space Sciences, University of Michigan, Ann Arbor, MI, USA

Abstract

The SCintillation and Ionospheric Occultation NanoSat (SCION) mission deploys two CubeSat spacecraft in a close pearls-on-a-string orbital track to perform multipoint topside and limb occultation measurements of the ionospheric total electron content (TEC). Small-scale ionospheric density variations, or irregularities, are thought to be the source of transionospheric signal degradation, known as ionospheric scintillation. Scintillation has traditionally been associated with the equatorial and polar ionosphere. However, scintillation may occur at mid-latitudes along the steep density gradients associated with geomagnetic Storm Enhanced Density (SED) regions. As our technological society grows increasingly connected and reliant on space-based communication and navigation systems, a growing number of users are susceptible to mid-latitude scintillation. Meanwhile, CubeSats and commercial dual-frequency GPS receivers have developed sufficient flight heritage and capability to compose a low-cost, small satellite multipoint mission to observe small-scale density irregularities in the ionosphere. The SCION mission investigates mid-latitude density variability and associated signal scintillation by making simultaneous multipoint observations of the ionospheric TEC using an onboard dual-frequency GPS receiver. SCION will also measure the GPS L1 carrier-to-noise ratio to compute the S4 amplitude scintillation index corresponding to the observed density irregularities observed in TEC. Comparisons between observations from each spacecraft enable the study of small-scale ionospheric density structure, particularly irregularities, that are associated with ionospheric scintillation and the degradation of space-based navigation and communication systems.

1. Introduction

1.1. Motivation and Background

Space weather events strongly influence variations in the ionosphere's density structure (Prikryl et al., 2010), and radio signals transiting the ionosphere are especially susceptible to adverse effects of this variability. Perhaps the most disruptive of these effects is the diffraction and scattering of radio signals known as ionospheric scintillation. Radio frequencies transmitted from space to the ground can experience

Corresponding Author: Thomas R. P. Heine, heinet@umich.edu

scintillation when they encounter variations in ionospheric electron density on the size of the Fresnel radius, given by Equation 1 below (Ledvina et al., 2002), where λ is the signal wavelength and z is the closest distance from the ionospheric irregularity to the receiver (~300 km typically for most users).

$$\mathrm{R_{Fresnel}}\sqrt{\lambda z} \quad (1)$$

Small-scale (~1 km) variations (or irregularities) in ionospheric electron density correspond to the Fresnel radius of radio frequencies between 100 MHz – 3 GHz. Consequently, small-scale irregularities can have a dramatic effect on satellite-based communication and navigation systems that often operate in this frequency range. User impacts can range from degradation of the received signal strength and dropped data packets, to the complete inoperability of these systems (Datta-Barua et al., 2003).

The scale, structure, and frequency of occurrence of small-scale irregularities are some of the key questions in ionospheric scintillation research, though scintillation is typically thought to be infrequent in the mid-latitude ionosphere, as illustrated in Figure 1 by Basu and Groves (2001). However, during geomagnetic storms, regions of enhanced ionization are increasingly observed in the American Sector beginning at equatorial latitudes, stretching poleward and towards noon across mid-latitudes, with similar enhancements observed beginning at higher latitudes in the European and Asian Sectors (Yizengaw et al., 2008; Zou et al., 2014). These storm enhanced density (SED) regions (see Figure 2) have steep density gradients along their flanks that can produce a cascade of small-scale density structure (irregularities) and a worsened scintillation environment (Foster, 2005). Understanding how and when small-scale density structures and GPS scintillation at mid-latitudes form and evolve under the influence of space weather events is an open science question that would improve our understanding of space weather effects on technology and society. Answering these questions requires further detection and observation of these structures.

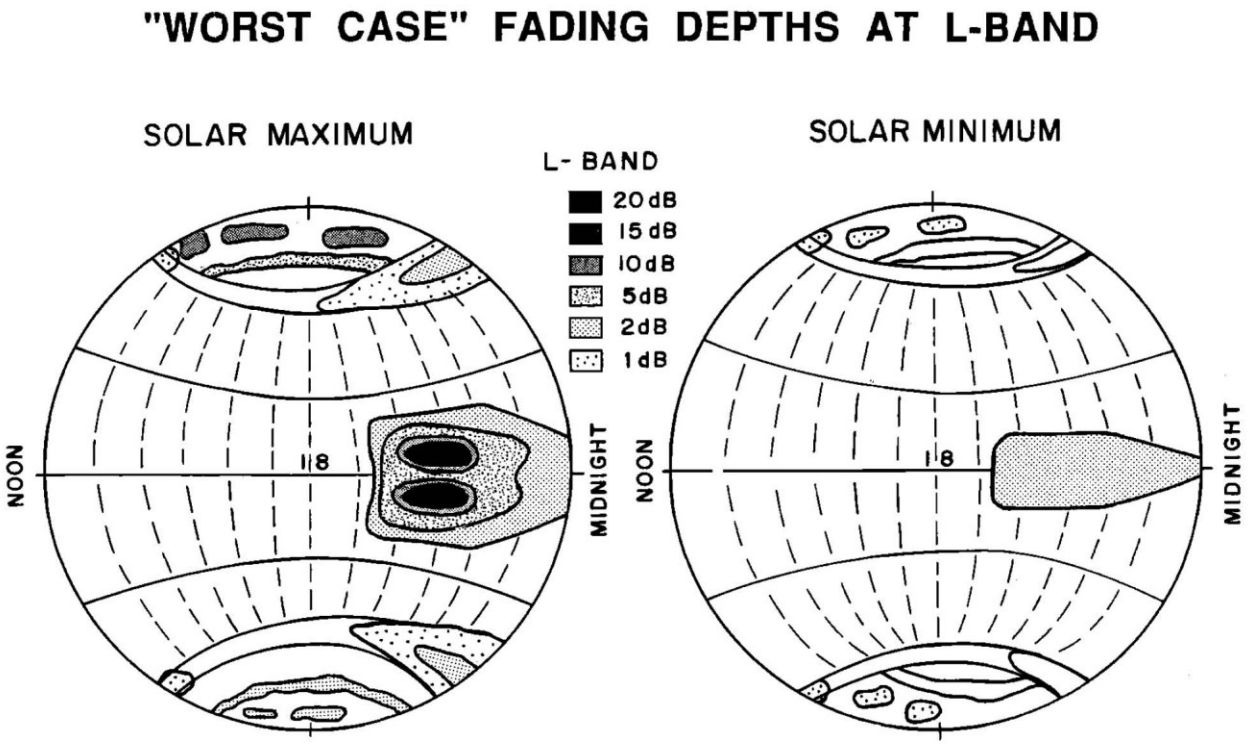

Figure 1. Schematic representation of global scintillation effects for L-band frequencies during solar maximum (left) and minimum (right) Basu and Groves (2001). Notice the absence of L-band scintillation at mid-latitudes.

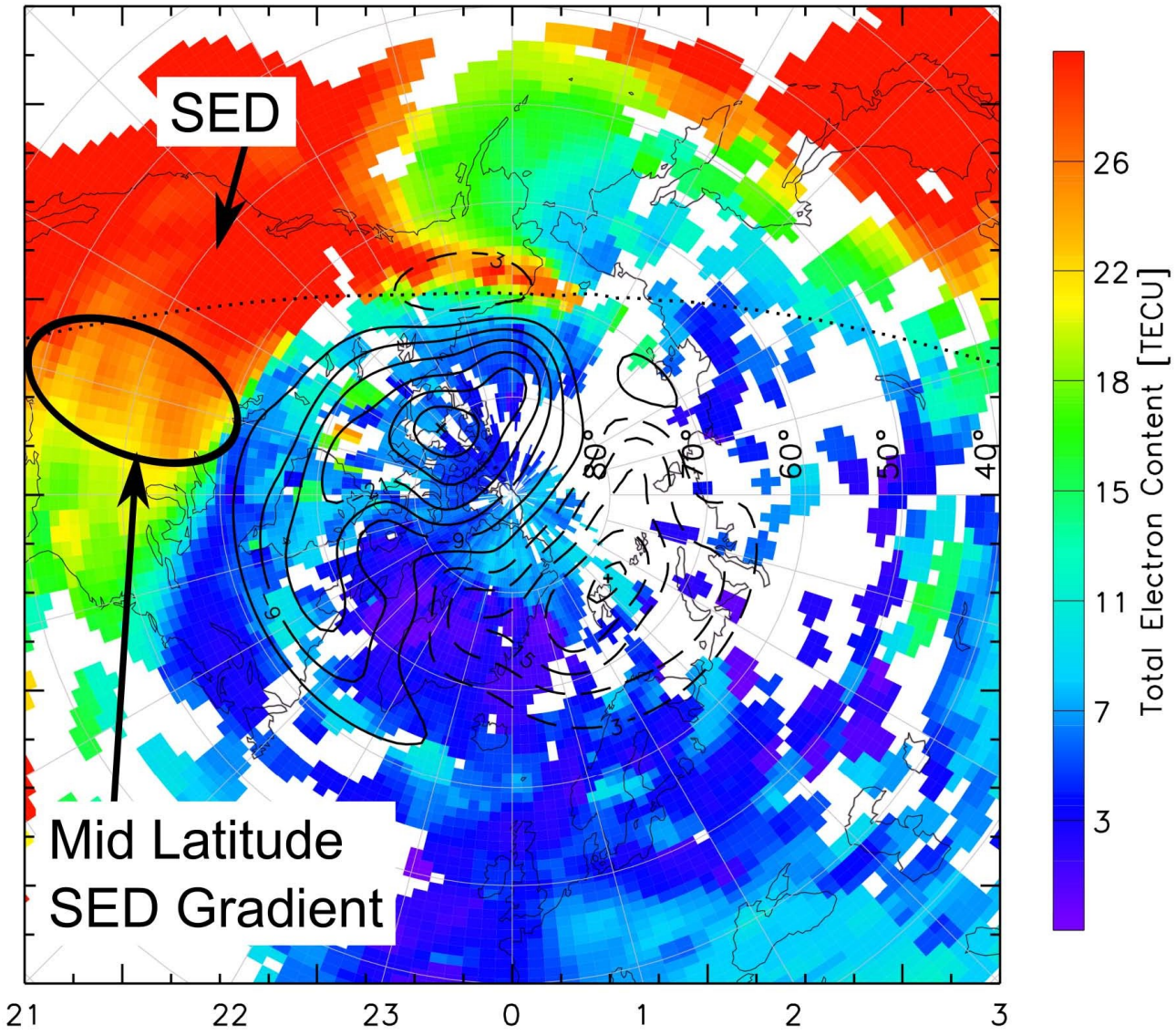

Figure 2. Polar view of November 14, 2012 SED over North America indicated by ground-based TEC (Zou et al., 2014). SCION will investigate density irregularities and scintillation formed along the gradients of large scale mid-latitude density structures such as these.

1.2. Previous Work

There are several ground-based methods for observing ionospheric density structure (Zou et al., 2013). Ionosondes, radar, and GPS total electron content (TEC) can produce vertical measurements of density, but are limited by the relatively small number of stations and limited coverage areas, especially over the oceans. Ionosondes are further limited to measurements below the height of the ionosphere's maximu electron density—the F peak. Sounding rockets can provide in situ density measurements at high temporal and spatial resolution, but they are limited to localized observations and short flight durations. Space-based measurements of ionospheric density structure allow long duration observations, expand the coverage area, including over the oceans, and allow for unique measurement geometries not possible from the ground, such as horizontal TEC used in constructing vertical density profiles (Hajj and Romans, 1998) and topside TEC that measures ionospheric densities above the F Peak (Yizengaw et al., 2005).

Furthermore, small-scale irregularities are especially difficult to detect from ground-based TEC observations. While incoherent scatter radars (ISR) are capable of detecting them, there are only a small number of such facilities around the world. Consequently, the Rate of Change in TEC Index (ROTI) (Pi et al., 1997) has been used to infer the presence of mid-latitude density irregularities on the order of several kilometers in scale over broad regions. This method assumes that irregularities are steady structures on the timescale in which they drift past the GPS raypath and measurements are made at 30-second intervals. The raypath from a GPS satellite with a 12 hour period moves through the F region at velocities ~30–400 m s^{-1}, and ion drift velocities at mid-latitudes have been detected by Millstone Hill radar at 200–1000 m s^{-1} (Sun et al., 2013), while the observed density variation is attributed to the drift of stable density structures. Consequently, for low and mid-latitudes, the size of irregularities that have been reliably detected with this method is only a few kilometers. Recently, Sun et al. (2013) combined ROTI with an improved filtering algorithm to resolve TEC gradients on the order of a few degrees latitude in scale (~100 km) from TEC maps of the continental United States. The ROTI calculated from TEC data was then superimposed on the filtered TEC gradients. Sun et al. (2013) suggest that regions of high ROTI in the vicinity of larger gradients may be due to the formation of small-scale irregularities under drift-dependent instability criteria. However, since the ROTI can be attributed to either the size or the drift of these structures, some ambiguity remains in confirming the occurrence of small-scale irregularities in the vicinity of SED regions. What is needed is the detection of scintillation causing small-scale irregularities that can separate spatial and temporal variation, such as possible with the SCION multipoint mission.

Variability of the ionosphere's density structure was also investigated by the Dynamic Ionosphere Cubesat Experiment (DICE) twin CubeSat formation. DICE measured density structure using in situ Langmuir probes in an eccentric orbit of 456 x 808 km at 101° inclination. Consequently, density observations were limited to the local plasma environment. In addition, without spacecraft separation control, DICE did not maintain the close formation necessary for resolving spatial and temporal ambiguity at the ~1 km scale (Crowley et al., 2011). DICE's variable separation, eventually separating to >300 km between spacecraft, allowed it to make in situ measurements across a range of spatial scales. However, the variable separation combined with in situ measurements precluded focused and broad observation of small-scale structure across a range of geomagnetic activity. The COSMIC mission launched in 2006 made multipoint occulted and topside GPS TEC measurements, along with measurements of GPS scintillation; however, COSMIC's observations were tens of kilometers and several minutes apart. Unfortunately, since COSMIC was designed for global coverage as an operational mission, its spacecraft also did not maintain the close formation geometry required for continued multipoint observations (Anthes et al., 2008; Fong et al., 2007; Brahmanandam et al., 2012). SCION seeks to extend the period of irregularity observation for small-scale multipoint observations <5 km, and continue multipoint TEC and scintillation observations through the remainder of the one year mission.

2. SCION Mission Overview

SCintillation and Ionosphere Occultation NanoSats (SCION) is a CubeSat-based mission specifically designed to make multipoint, GPS TEC and scintillation observations of the ionosphere on the spatial scales associated with communication and navigation system degradation. SCION especially focuses on the mid-latitude ionosphere where small-scale irregularities can form along the boundaries of larger, meso-scale gradients, such as those that form along storm enhanced density (SED) regions (Foster, 2005). To do so, SCION takes high-rate (1–50 Hz) TEC and amplitude scintillation measurements using commercially available dual-frequency GPS receivers onboard two low-Earth-orbit (LEO) CubeSat spacecraft. Combining TEC and scintillation allows SCION to detect and quantify small-scale structure near larger ionospheric gradients. The separation between the spacecraft achieves two simultaneous, in-

dependent measurements of TEC per GPS spacecraft in view, that can be used to infer ionospheric electron density structure. Early in the mission, these spacecraft will be in close proximity and gradually separate over the one year mission lifetime, spanning a range of ionospheric spatial scales. The TEC observations are also used to measure vertical density profiles that are important for the quantification of the background large-scale density structure. Meanwhile, the multipoint scintillation measurements help to define edges of scintillating regions and locate regions of small-scale irregularities not directly detected in TEC variations by the two spacecraft. SCION is the first multipoint LEO GPS TEC mission dedicated to investigating the formation and evolution of scintillation causing small-scale density structures at mid-latitudes along the boundaries of SED regions.

2.1. Science Measurements

2.1.1. GPS Total Electron Content

TEC is the integrated electron number density, n_e, along a given raypath between points s_1 and s_2 given by Equation 2. The phase velocity of a signal traveling through a plasma (such as the ionosphere), depends on the plasma's electron density. Equation 3 gives the phase velocity for an electromagnetic wave of frequency f in a plasma (Chen, 1984) where v_ϕ is the wave phase velocity, ω_p is the plasma frequency (given by Equation 4), m_e and e are the mass and charge of an electron respectively, and c is the speed of light. From Equations 3 and 4, it can be seen that the wave propagation speed is dependent on its frequency and the plasma electron density.

$$\mathrm{TEC} = \int_{s_1}^{s_2} n_e \, ds \tag{2}$$

$$v_\phi^2 = c^2 + w_p^2 \frac{f^2}{c^2} \tag{3}$$

$$\omega_p^2 = \frac{n_e e^2}{\epsilon_0 m_e} \tag{4}$$

Because radio signals of different frequency travel through the ionosphere at different speeds, the slight difference in transit time between the GPS L1 and GPS L2 frequencies, 1575.42 MHz and 1227.60 MHz respectively, can be used to infer TEC between the transmitting GPS satellite and the receiver. Mannucci et al. (1993) gives Equation 5 as the relationship between the GPS L1 and L2 pseudorange delay and TEC.

$$\mathrm{TEC} = (P_1 - P_2) \cdot 2.852 \times 10^{16} \quad [e \cdot m^{-2}], \tag{5}$$

where P_1 and P_2 represent the pseudorange transit time in nanoseconds measured from the GPS L1 and L2 signals, respectively. Each SCION spacecraft records the pseudorange delay of both GPS frequencies, which are used to compute TEC along the observation raypath.

2.1.2. The S4 Amplitude Scintillation Index

Measurements of GPS amplitude scintillation also help to detect the presence of small-scale irregularities not detected in TEC measurements directly. SCION computes the S4 amplitude scintillation along the observation raypath using the received carrier-to-noise ratio (C/N_0) as a proxy for signal power. The S4 index is computed for both frequencies according to Equation 6 (Van Dierendonck et al., 1993), where I is the signal power and the angle brackets $\langle\ \rangle$ represent the average over a 60 second interval.

$$\mathrm{S4} = \sqrt{\frac{\langle I^2 \rangle - \langle I \rangle^2}{\langle I \rangle^2}} \tag{6}$$

2.2. Measurement Geometry

SCION's two spacecraft target observations of small-scale ionospheric irregularities <5 km in size for at least the first three months of the mission. Observations will be in three measurement geometries: topside, side scanning, and limb occultation, which observe different regions of the ionosphere. Since at any given time, there are GPS satellites in one or more of these measurement geometries, all line-of-

sight accesses to the GPS constellation are potentially valid observations. These measurement geometries are shown in Figure 3.

2.2.1. Limb Occultation

Rearward looking limb occultations (Figure 3, shown in green) produce vertical density profiles of the ionosphere while tracking GPS satellites as they set behind the local horizon (Hajj and Romans, 1998) relative to SCION. Setting satellites are preferred for limb occultation over rising satellites because they have already been acquired by the GPS receiver and do not require lose time while acquiring a new signal lock before making measurements, which can take up to ten seconds. The vertical distance between samples in a vertical profile depends on the direction and relative velocity between the GPS satellite and SCION. The relative velocity can then be attributed chiefly to the motion of SCION, since its orbital velocity is much faster than the GPS satellites, which can be considered stationary when estimating the vertical resolution of a limb occultation profile. Analysis shows a GPS satellite setting directly behind SCION sampled at 1 Hz produces ionospheric profiles in ~150 m increments.

2.2.2. Topside VTEC

SCION also measures the topside vertical TEC (VTEC) of the ionosphere (Figure 3, shown in red). The local VTEC is measured by mapping the slant TEC within a 20° half-angle cone around zenith to the local vertical. The topside region is of special interest because it connects the low altitude dense regions of the ionosphere to the inner edge of the plasmasphere. Topside TEC measurements isolate the density structure of the topside ionosphere and plas-

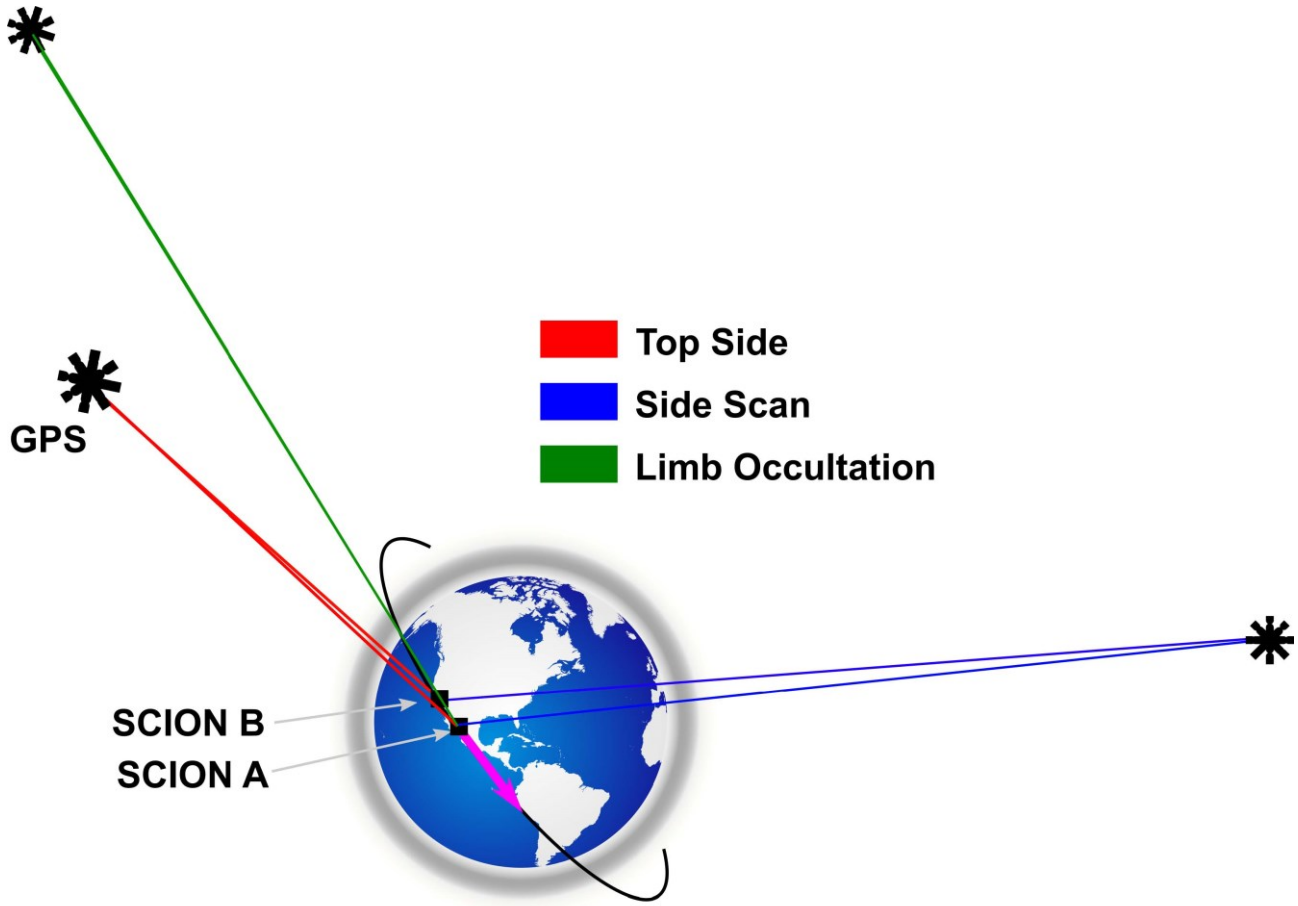

Figure 3. The two SCION spacecraft follow the same orbit with their velocity vector indicated in magenta. Measurement Geometries: Rearward limb occultation (green), topside VTEC (red), and side-scan in-situ (blue). (Earth image credit: VectorTemplates.com)

masphere up to the GPS altitude at 4.2 R_E. Small scale structure at these altitudes are not easily resolved against the dense F region in ground-based TEC measurements, so topside measurements can only be made from spacecraft. This measurement also lends itself to tomographic inversion of the topside density structure by inverting the structure from multiple slant TEC measurements, similar to the structure in Figure 4 constructed by Yizengaw et al. (2006) from FedSat LEO measurements.

2.2.3. Side Scanning Near Field

SCION also measures variations in local ionospheric density near the two SCION spacecraft by observing low-elevation GPS satellites in the cross-track direction (Figure 3, shown in blue). In this case, the relative vertical velocity of the GPS satellite is negligible and observations are at nearly constant altitude. One of the challenges in performing ionospheric occultation from a single spacecraft is the double crossing through the ionosphere's F peak for any single raypath between GPS spacecraft and the observing spacecraft. Unlike the neutral atmosphere where density decreases with altitude, the ionosphere has a high density band (the F Region) that peaks around 300 km during geomagnetic quiet times. Consequently, any given raypath during an occultation intersects this dense band at two "pierce points" due to the curvature of the Earth (Tsybulya and Jakowski, 2005), and it is nearly impossible to distinguish the TEC contribution of each F peak crossing. With two spacecraft, however, this becomes much easier. Since the SCION spacecraft are several times closer to the

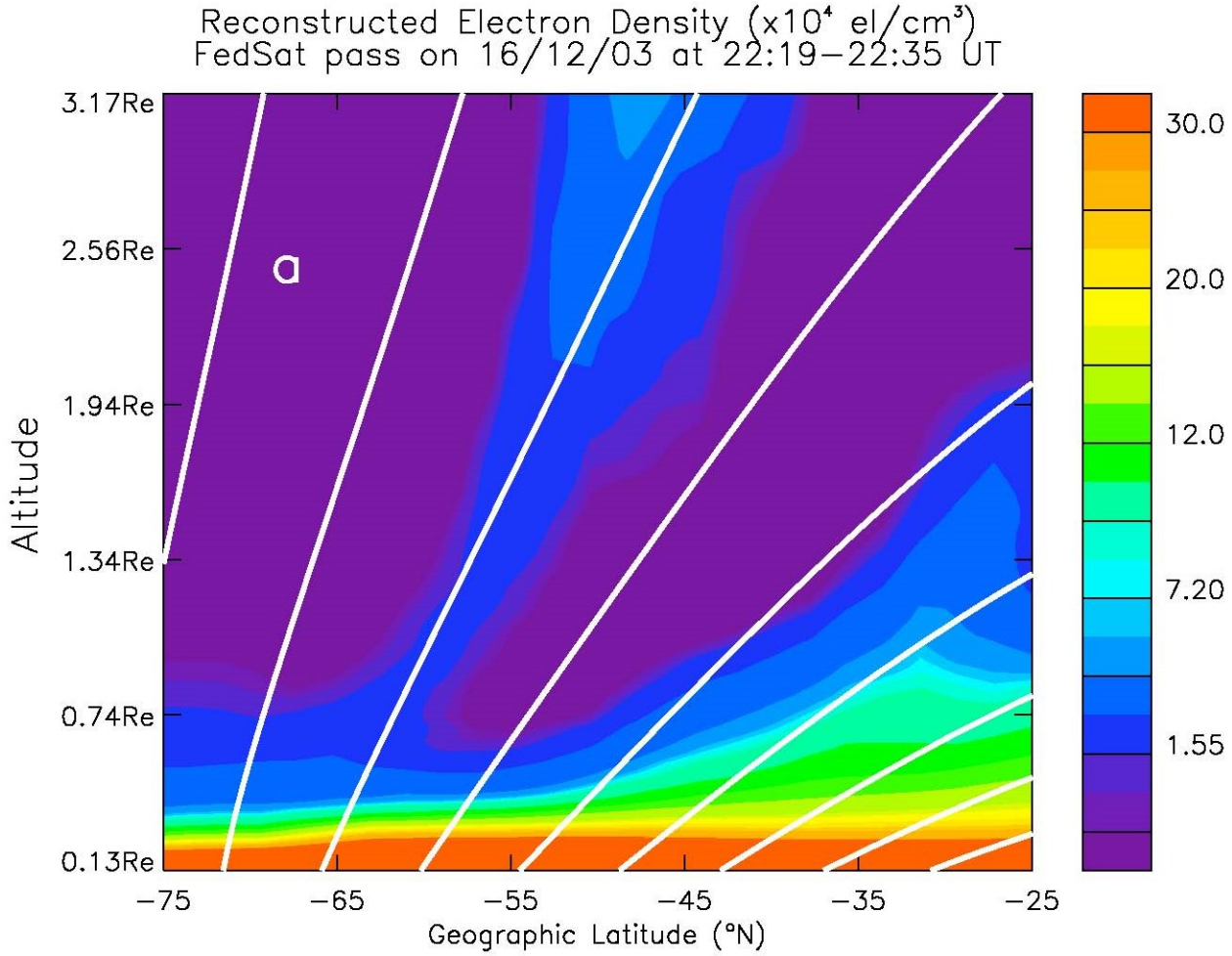

Figure 4. Tomographically reconstructed vertical density profiles FedSat slant TEC measurements (adapted from Yizengaw et al. (2012)).

near pierce point than the far pierce point, it is reasonable to assume both ray paths effectively observe nearly the same density at the far pierce point. In this case, any observed TEC variations observed in the side scanning geometry can be attributed to the near pierce point. Therefore, in this configuration, SCION measures TEC gradients in the near field, similar to an in-situ measurement at the near pierce point. The left panel of Figure 5 shows in situ electron density measurements made by DMSP spacecraft when crossing SED boundaries. SCION's side scanning geometry will be used to produce analogous measurements of the near field density structure.

3. Mission Design

Preliminary spacecraft design work for SCION was completed by Space Systems Master of Engineering students as part of the space systems design curriculum of the University of Michigan's Atmospheric, Oceanic, and Space Sciences program. This section outlines the spacecraft and subsystem sizing that demonstrates the feasibility of the SCION mission.

3.1. Concept of Operations

SCION's mission objectives are well-suited to the focused and highly cost-effective nature of CubeSat missions. Many of SCION's subsystems benefit from previous CubeSat missions, and SCION itself belongs in a pipeline of CubeSat development at the University of Michigan. SCION consists of two identical CubeSat spacecraft that launch as a secondary payload and are ejected from a Poly PicoSatellite Orbital Deployer (PPOD) at an orbit determined by the

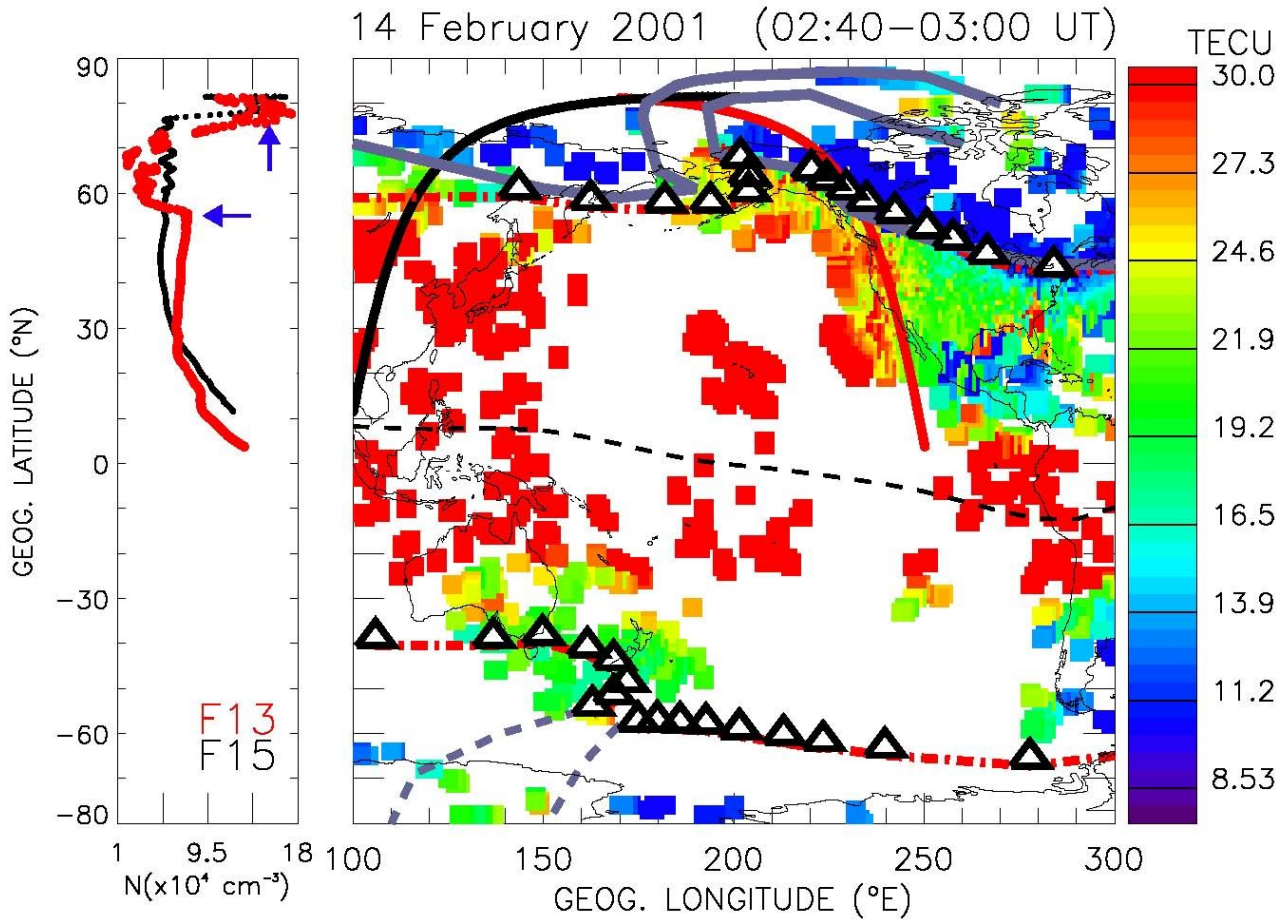

Figure 5. Right: GPS TEC map showing a SED plume in the North American sector. The white triangles correspond to the magnetic footprints of the plasmapause as observed by IMAGE EUV. Left: Two in situ density measurements observed by DMSP F-13 and F-15 at ~870 km altitude (Yizengaw et al., 2008).

specific primary launch vehicle payload, but desired within 500–600 km and 40° and 60° inclination as described in Section 3.3. The 1U spacecraft each feature two fixed, deployable solar arrays 10 × 10 cm in size, and a deployable tape-measure whip antenna tuned to ~437 MHz for uplink and downlink communication. The solar arrays and antenna will autonomously deploy no earlier than 30 min after ejection from the PPOD per CubeSat Design Specification Rev 13, (Pignatelli and Mehrparvar, 2014). The two spacecraft will begin the mission while in contact with one another, and with nearly zero ΔV difference at ejection from the PPOD. They are allowed to drift freely while being gradually separated by aerodynamic forces. The separation rate will be minimized to extend the duration the two spacecraft are able to make observations between 0.2 and 5 km, which is expected to be at least three months from ejection. The spacecraft separation concept is described further in Section 3.3.4. SCION uses a "store-and-forward" data delivery system. Science data and housekeeping telemetry will be downloaded per ground command to a single dedicated ground station in Ann Arbor, Michigan. The minimum success lifetime for the SCION mission is six months, with a goal of one year.

SCION has five operational modes: Safe, Detumble, Deploy, Standby, and Science Operations. The spacecraft are in Safe Mode immediately following ejection from the PPOD, and are returned to that state automatically after an anomalous restart. During Safe Mode, only the flight computer, power system, and communication uplink system (in standby) are active. Detumbling occurs after ejection, actively using coarse attitude sensors and magnetic torquers prior to deployment of the solar arrays and communication antenna. During detumbling, there is a slight battery charging deficit accumulating 5.5% per orbit until the solar arrays are deployed. Detumbling is expected to be accomplished within two orbits. Deployment is identical to Safe Mode, but includes powering the release mechanisms to deploy the solar arrays and communication antenna. Standby Mode is similar to Safe Mode, but requires a command from the ground to initiate (typically out of Safe Mode). It includes uplink and downlink communication and attitude sensor monitoring. Lastly, the Science Operations Mode adds the activation of the GPS receiver science payload, and performs active attitude determination and control.

3.2. Science Payload

Each of the two SCION spacecraft will carry either a Novatel OEMV-1DF or a Septentrio AstRx-m GPS receiver. These receivers have lower cost, mass, and a better form factor for CubeSat applications when compared with other dual-frequency receivers that have flown in space, such as the Broad Reach/JPL BlackJack receiver (Dyrud and Fentzke, 2011). The final receiver selection will be determined by ongoing testing. Performance tests were done with an OEMV-2, which is functionally identical to the OEMV-1DF. The OEMV-1DF has a compact form factor (7.1 × 4.6 cm) that fits well on a conventional 1U CubeSat board stack and, in its single-frequency version, has flight heritage on RAX and RAX-2 (Arlas and Spangelo, 2013). The OEMV-1DF is capable of sampling up to 50 Hz and consumes 1.3 W of power. The AstRx-m, manufactured by Septentrio Satellite Navigation, is a lightweight, small form factor GPS receiver capable of sampling the GPS constellation at up to 50 Hz. The dominant advantage of the AstRx-m is that it only consumes 0.5 W during operation. Further testing will inform the final payload selection from these two receivers.

SCION's GPS antenna configuration is designed to ensure a minimally obstructed view of the GPS constellation and maximize the opportunity for observations without the need for precise attitude determination and control. Each SCION spacecraft will have two dual frequency GPS patch antennas mounted on opposite (+/−X) faces of the CubeSat. Since each antenna has a 100° field of view for both frequencies, the spacecraft will slowly rotate about the Z axis. A baseline rotation rate of 0.3 RPM was chosen because it ensures that a GPS spacecraft crossing the antenna center has at least 60 s within the 3 dB gain peak. This is followed by 48 s where the GPS satellite falls outside of this range before being reacquired via the second antenna. The Novatel OEMV-2 testing showed that individual GPS satellites reacquire L1

lock within 2 s, and L2 in within 8 s. It is likely the receiver is able to maintain lock at elevation angles outside of the 100° 3 dB gain pattern, which would further expand the opportunity for observations. This will be confirmed in future tests, but for the present analyses, observations were limited within a 100° field of view.

3.3. Orbit Selection

SCION's orbit should maximize the opportunity for observations of the mid-latitude ionosphere, which is quantified by the frequency of access to the GPS constellation while SCION is below ±60° latitude. This condition is valid for observing the mid-latitude ionosphere because the distance from SCION to the F-peak during side scanning observations is within ~6°, latitude or longitude, putting most observations at mid-latitudes (Figure 6). There are three additional constraints that inform orbit selection. First, the orbit shall allow a minimum mission lifetime of six months (with a goal of one year), while not exceeding the provisions of NPR 8715.6A (2009), which requires deorbit within 25 years of end-of-mission. Second, the orbit should maximize the number of daily accesses to the University of Michigan ground station in Ann Arbor. Third, the altitude shall allow observations at the desired spatial scale for at least 90 days. Though the orbits used for this analysis are all circular, circular orbits are not required, and the suitability of eccentric orbits would be similarly analyzed given such a launch opportunity.

3.3.1. GPS Constellation Access

The opportunity for observation of the mid-latitude ionosphere depends on the frequency and duration of access to the GPS constellation. While all line-of-sight accesses to the GPS constellation are potentially valid observations within the three measurement geometries of topside, side scanning, and limb occultation, orbits were assessed on the average total daily access time to GPS spacecraft below the SCION local horizon. Since SCION is above the ionosphere's densest altitude, accesses below the local horizon have the best opportunity to observe F region irregularities. To estimate the observation opportunity possible with different orbits, the Systems Toolkit (STK) by Analytic Graphics Inc. was used to compute the cumulative access time to the GPS constellation over a one year time period, shown in Figure 7. For this analysis, the spacecraft was assumed to be +Z northward pointing with two 100° beam width antennas, pointing in opposite directions perpendicular to the spin axis, and a rotation rate of 1 RPM. With slower spin rates, access time increases linearly, independent of altitude and inclination. The orbits analyzed were circular inclined orbits from 20° to 80°, and between 400 and 800 km. From Figure 7, it is clear that higher orbits provide greater access to the GPS constellation, suggesting that higher orbits allow more GPS satellites into view that would otherwise be obscured by the Earth. Furthermore, mid-latitude inclinations provide more constellation access than low or polar inclinations, since the GPS constellation itself is at 55° inclination. This analysis shows that 40° inclination would provide the greatest GPS access at most orbit altitudes and 60° provides the next best access opportunity up to 650 km. 50° inclination showed less, but comparable average daily GPS access time to 60°. There was also comparable access time at 30°, but with insufficient coverage of the mid-latitudes.

3.3.2. Ground Station Access

SCION will be operated from a single ground station at the University of Michigan in Ann Arbor, which is capable of communicating with multiple spacecraft simultaneously (described further in Section 3.4.4). More ground stations would be beneficial, but were not included in this study due to cost and use constraints. Total ground station access is a key factor in orbit selection, because SCION produces a large volume of data. Since ground station access is intermittent, SCION will not provide realtime science data; instead, it will store and forward data collected over one or more orbits. Orbit selection is further constrained by the requirement that all of SCION's data be downlinked by the end of the mission. This

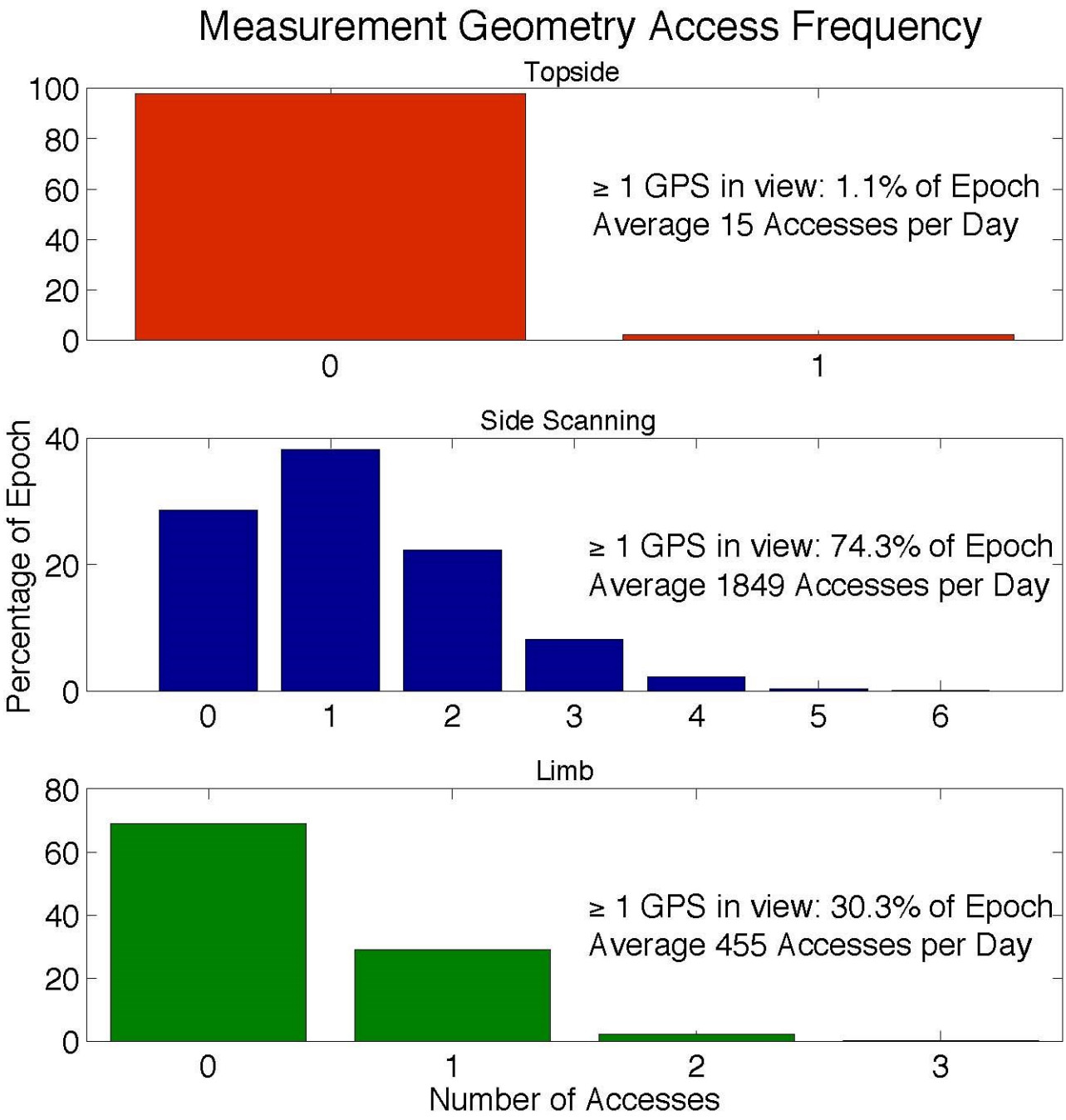

Figure 6. Typical number of GPS spacecraft within each of the three measurement geometries over a one-month epoch of mission time.

requirement allows for temporary lags in data transmission, and requires only average ground station access times, rather than placing unnecessarily stringent requirements on day-to-day access, which can vary considerably. Potential SCION orbits were analyzed in STK over one year to determine the average daily contact time for several inclinations and altitudes, for a period of one year. Only circular orbits were analyzed. Figure 8 indicates that inclinations between 40° and 60° provide the greatest average access time for altitudes below 700 km, and inclinations between 50° and 70° above 700 km.

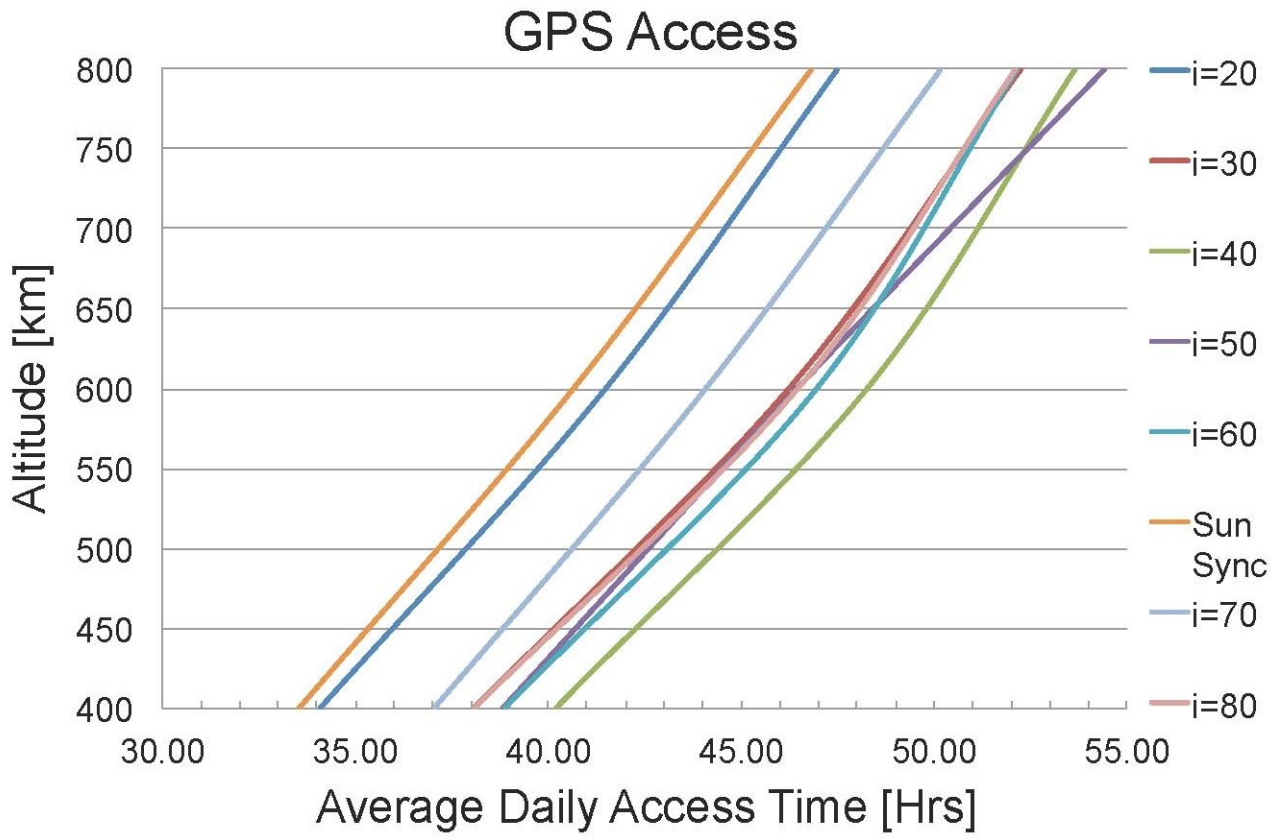

Figure 7. One year access time to the GPS constellation below SCION local horizon in one day averages. The accesses were modeled with two 100° FOV antennas, and Z axis rotation at 1 RPM.

3.3.3. Mission Lifetime

The minimum SCION mission lifetime is six months, with a desired lifetime of one year. The minimum lifetime of six months, allows for spacecraft checkout, formation separation, an operational duration sufficient to observe several SED events (Yizengaw et al., 2008). In addition, SCION's total orbital lifetime must be less than twenty-five years from the end of the operational mission. This requirement is a condition of the *CalPoly CubeSat Specification* (Req. 2.4.5) levied on all CubeSat missions (Pignatelli and Mehrparvar, 2014) and inherited from *NASA Procedural Requirements for Limiting Orbital Debris*, Requirement 56876 (NPR 8715.6A, 2009; NASA-STD-8719.14A, 2012). Representative orbits between 400–700 km, and 40° inclination were propagated in STK using the High Precision Orbit Propagator (HPOP) for a 1U CubeSat (1.33 kg) with a 2.2 drag coefficient. The atmospheric density was estimated from the U.S. Naval Research Laboratory MSISE-2000 atmospheric model (valid up to 1000 km), using the predicted solar 10.7 cm radio flux $F_{10.7}$ and $\langle F_{10.7} \rangle_{81\ \mathrm{Day}}$ [$(10)^{-22}$ W m^{-2} Hz^{-1}] and geomagnetic (Kp and Ap) conditions with a three-hour update rate from the Space Weather Data file by Celestrak and the Analytical Graphics Inc. Center for Space Standards and Innovation. The STK lifetime tool was used to calculate the lifetime of altitudes at 400, 500, 550, 600, 650, and 700 km, with effective drag areas of 0.01 and 0.34 m^2 representing the minimum and maximum possible effective drag areas. The results of this analysis, shown in Figure 9, suggest that orbits below 450 km will not meet the six-month lifetime requirement for minimum success, whereas orbits above 600 km will exceed the 25-year limit. These conditions propagated at 40° and 60° inclination produced the same result.

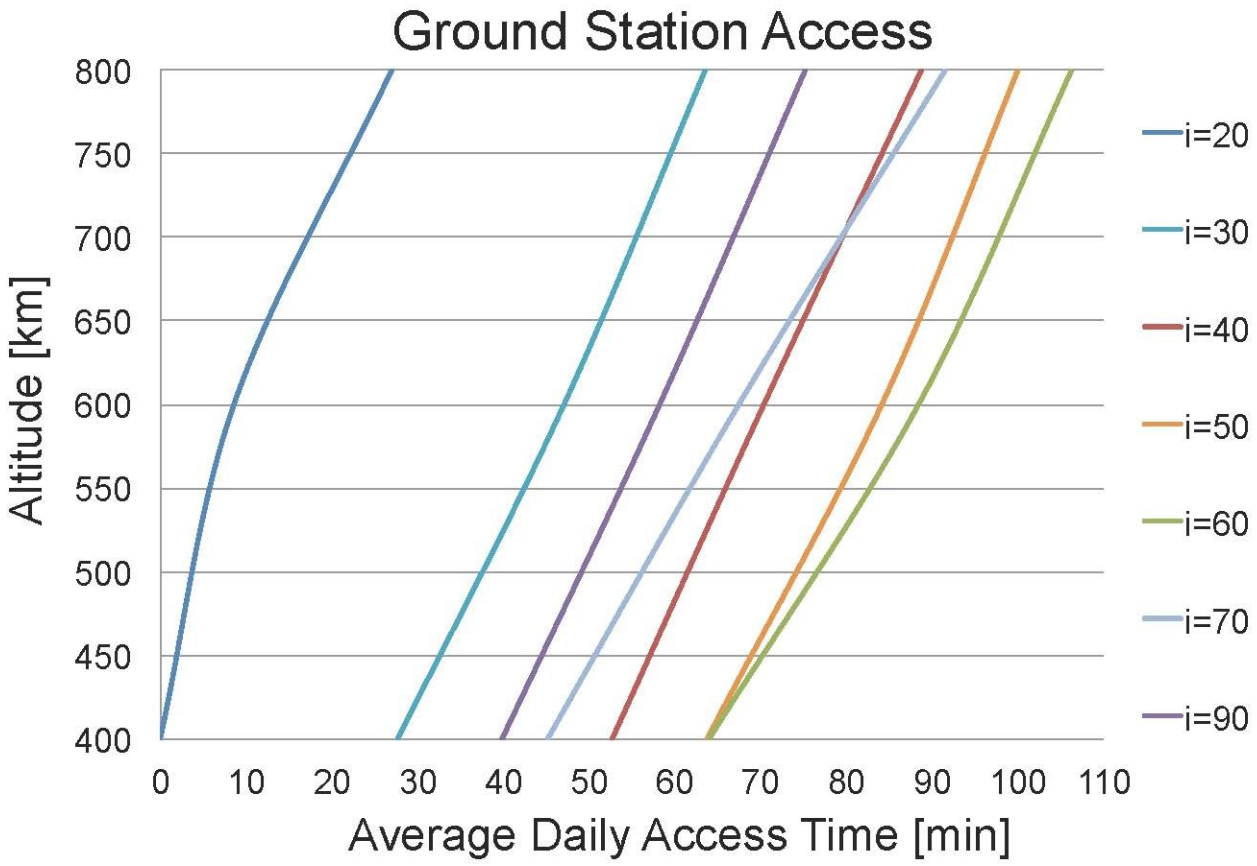

Figure 8. One year average daily access time to a ground station in Ann Arbor, Michigan, with near omnidirectional UHF whip antenna and Z axis rotation at 1 RPM.

3.3.4. Spacecraft Separation

Controlled separation between the two SCION spacecraft is one of the greatest challenges of the mission design. Upon deployment, the two SCION spacecraft are allowed to drift freely. Despite both CubeSats' initial deployment into the same orbit and position, there are three primary forces that can act to separate them. Additional forces, such as tides and gravitational variation, act equally on both spacecraft, and are therefore neglected (Sabol et al., 2001). The three primary forces affecting SCION spacecraft separation are: 1) the plunger springs required between CubeSats deployed from the same PPOD (Pignatelli and Mehrparvar, 2014); 2) the PPOD main spring that ejects the CubeSats; and 3) differential drag forces acting on the CubeSats depending on their orientation and any surface inconsistencies. Fortunately, the first two forces can be mitigated prior to launch. Per personal correspondence with the CalPoly CubeSat Program, the requirement for separation springs between the two SCION spacecraft can be waived, since they are a single mission. Relieving this requirement also mitigates the potential ΔV source of the PPOD main spring. Since the two SCION spacecraft do not have separation springs, they remain in contact with one another and the main spring acts on them equally as a single mass. The remaining ΔV source is the differential aerodynamic drag. Even though they are intended to be identical in shape, surface, and mass, the two SCION spacecraft may experience slightly different drag forces due to subtle surface inconsistencies or differences in orientation relative to the velocity vector. Initially, this differential drag force is desired to achieve separation, however if the separation rate is too fast, the amount of time spent within a useful range will be too short to achieve the science mission goals.

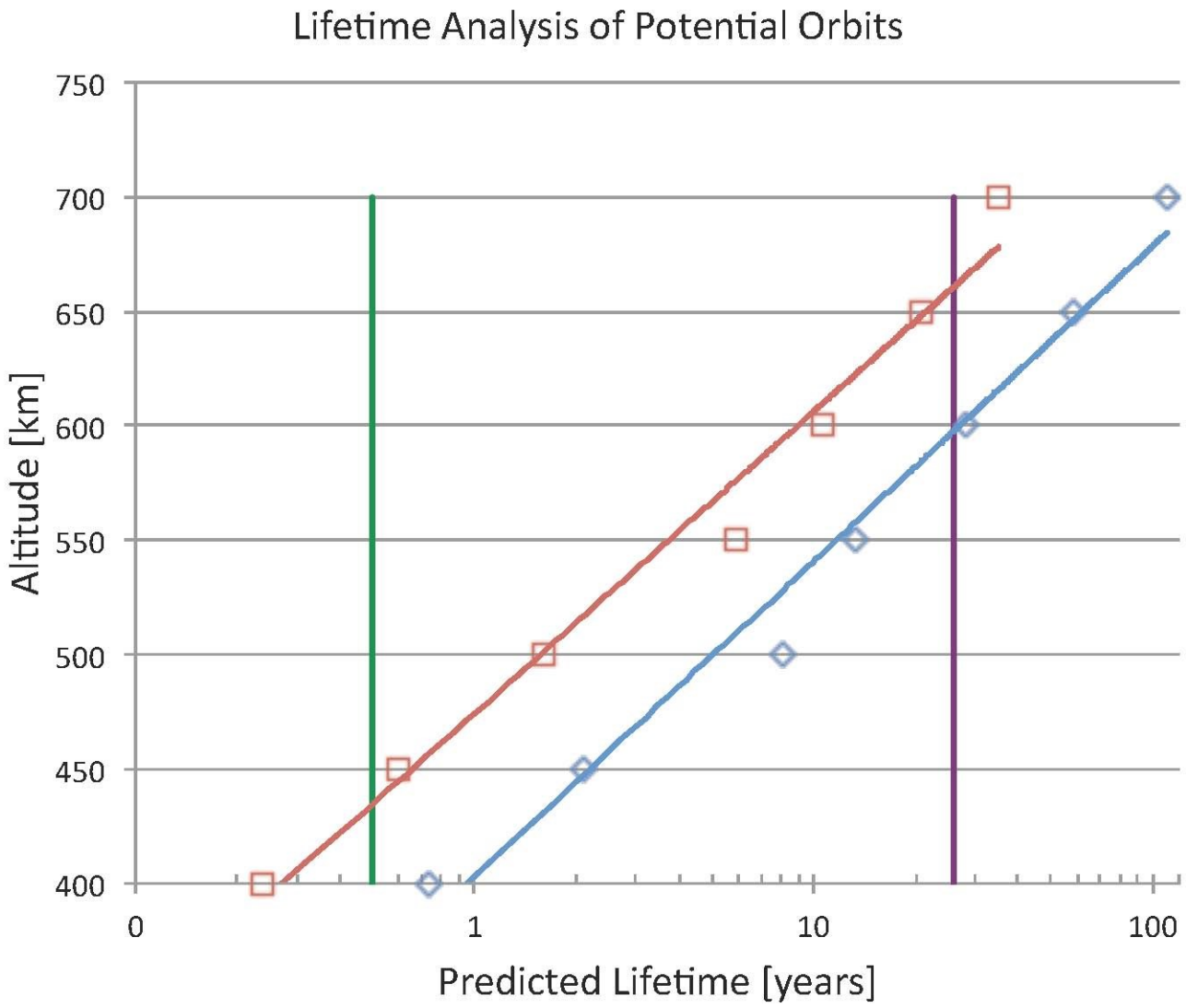

Figure 9. Predicted lifetime for SCION at 400–700 km circular, 40° inclined orbits. The red and blue lines indicate effective drag areas 0.010 m2 and 0.034 m2respectively. The green and purple vertical lines illustrate the 6-year minimum and 25-year maximum lifetime requirements respectively.

To address this question, SCION was modeled in STK using the NRLMISE-2000 atmospheric model for active, moderate, and quiet solar and geomagnetic conditions at altitudes of 500, 550, and 600 km. Active times were defined as having an $F_{10.7}$ and $\langle F_{10.7}\rangle_{81\ Day}$ of 200 with Kp of 6; moderate times, as $F_{10.7}$ and $\langle F_{10.7}\rangle_{81\ Day}$ of 120 and Kp 3; and quiet times, defined as $F_{10.7}$ and $\langle F_{10.7}\rangle_{81\ Day}$ of 90 and Kp of 3. These cases represent the extremes and typical conditions observed during the present and previous solar cycle. The two spacecraft were placed at the same point in space, holding the drag coefficient constant at 2.0, with a mass of 1.33 kg, and varying only their drag effective area by 1% from 251 cm^2, the RMS effective area for rotation about SCION's Z axis. The 1% difference in effective area was selected as the upper limit, based on simulations showing that higher effective area differences produced unsatisfactory separation rates. This approximately corresponds to the same area as the edge of an additional exposed 10 cm printed circuit board, or an 8.1° pitch difference between the two spacecraft. The basis of the other assumed parameters will be discussed in a later section. The two spacecraft's positions were propagated using

the STK Earth HPOP v8.1.1 propagator for one day, with the NRLMSISE-2000 atmospheric model set with the space environment parameters described above. Figure 10 shows the one-day line-of-sight separation between the two spacecraft after one day at quiet, moderate, and active conditions, with a 1% difference in effective drag area. This indicates not only the separation from initially matched positions and velocities, but also the differential ΔV in m day^{-1} that may occur over one day for a given space environment. Figure 10 also illustrates that a 50 km increase in altitude roughly halves the one-day separation. Since it is unlikely that any of these space environment conditions would be held constant over days or weeks, the spacecraft were again propagated in STK for 90 days using the same parameters as the one-day simulation, but using the predicted space-weather conditions for a 2015–2019 epoch (declining phase of the solar cycle) from the Space Weather Data file by Celestrak and the Analytical Graphics Inc. Center for Space Standards and Innovation. The environment was set to a three-hour update rate. The simulation results for 500, 550, and 600 km show a similar trend for separation distance increasing with altitude. Figure 11 shows that the simulated separation between the SCION for 600 km altitude after 90 days is ~8 km.

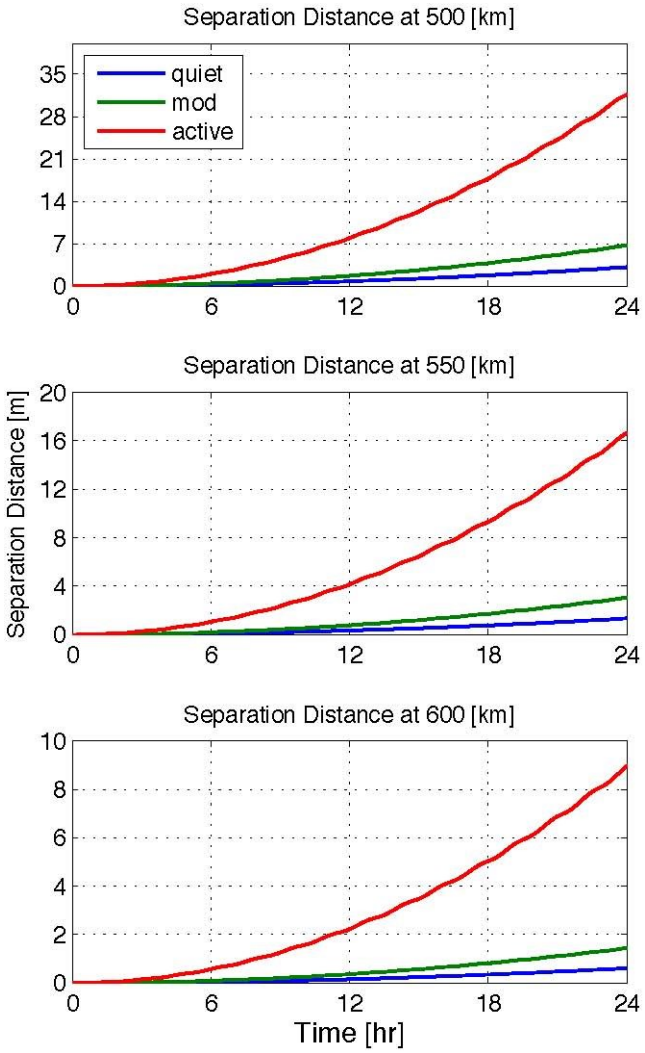

Figure 10. One-day separation in meters due to a 1% difference in effective drag area starting from matched positions and velocities. This also implies the one-day ΔV in m day^{-1} resulting from varying solar and geomagnetic conditions.

These simulations are based on several assumptions about the nature of the aerodynamic drag forces on the spacecraft and the characteristics of the spacecraft themselves. One of the primary assumptions in calculating spacecraft drag is that the drag force is proportional to the cross sectional area. Consequently, under this assumption, the orientation of a cube matters greatly. However, Hinch (1988) shows that for low Reynolds number flows, which are applicable here (Re <<1, Dalgarno and Smith (1962)), the drag force on a cube in uniform flow is independent of its orientation, and produces no net rotation. This makes intuitive sense, considering the stress tensor acting on a cubic surface is embodied in the drag coefficient, which differs, depending on whether the flow encounters a flat face or a pointed edge on the cube. Consequently, the product of C_d and A_{eff}, and the resulting drag force, remain approximately constant regardless of orientation. While the two SCION spacecraft are essentially cubes, they do have deployable solar panels and potentially other non-ideal surface features that violate this orientation independence. One way to reduce the effect of the non-idealized case is to rotate the two spacecraft along the same axis in near resonance. For two rotating spacecraft, the ratios of the RMS effective area over one period (of a reference spacecraft's rotation rate) remains within 1% if the second spacecraft rotation rate is within ~3% tolerance (or ± 6 s of the rotation period at 0.3 RPM) of a adjacent resonant mode of the reference spacecraft's rotation rate. At higher resonance modes,

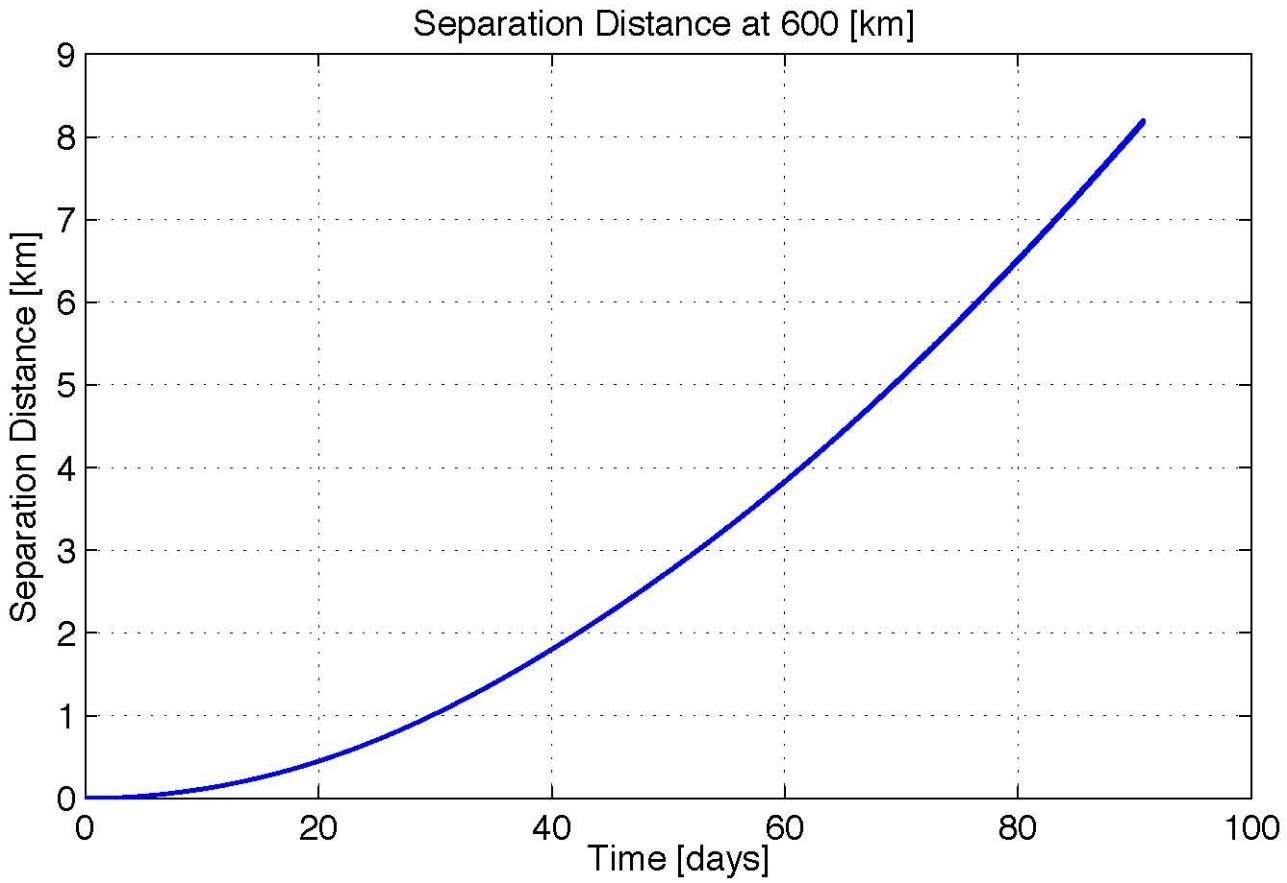

Figure 11. 90-day separation in kilometers due to a 1% difference in effective drag area at 600 km altitude.

the faster/slower relationship is reversed and the RMS effective area ratio for low rotation ratios rapidly exceeds 1%. The rotation's phase showed little or no effect for rotation rates on similar time scales. Figure 12 shows the ratio of effective areas with increasing differential rotation rates. A literature search of magnetorquer-controlled spin rates, including Sorensen (1971) and Damasceno Ferreira and Jaime Da Cruz (1991), suggests that implemention of spin control at this level does not exceed the capabilities of current CubeSat hardware.

Drag coefficients in the LEO regime are roughly bounded between $C_D = 2$ and $C_D = 4$ (Vallado and Fin-kleman, 2008). A drag coefficient of 2.0 was selected as a best case for the purpose of establishing feasibility. Since the drag force varies linearly with the drag coefficient, the resulting separation also scales linearly with C_D, and so the ~8 km separation with $C_D = 2$ could be as much as ~16 km for an extreme worst case $C_D = 4$.

Finally, an analysis was performed to determine acceptable separation distances. SCION's scientific goals are to observe ionospheric density structure on the scale associated with degradation of communication and navigation signals. Figure 13 shows the Freznel length spatial scales at relevant distances for LEO spacecraft and ground receivers. The analysis of the spacecraft separation rate shows this is not feasible 100% of the time. However, as the two spacecraft separate, the distance between their two line-of-sight ray paths does meet the desired spatial resolution for some observation angles. To determine how frequent the desired resolution is achieved for various spacecraft separation distances, a single spacecraft was modeled in STK with a 0.3 RPM rotation rate about a northward aligned spacecraft Z axis, and two

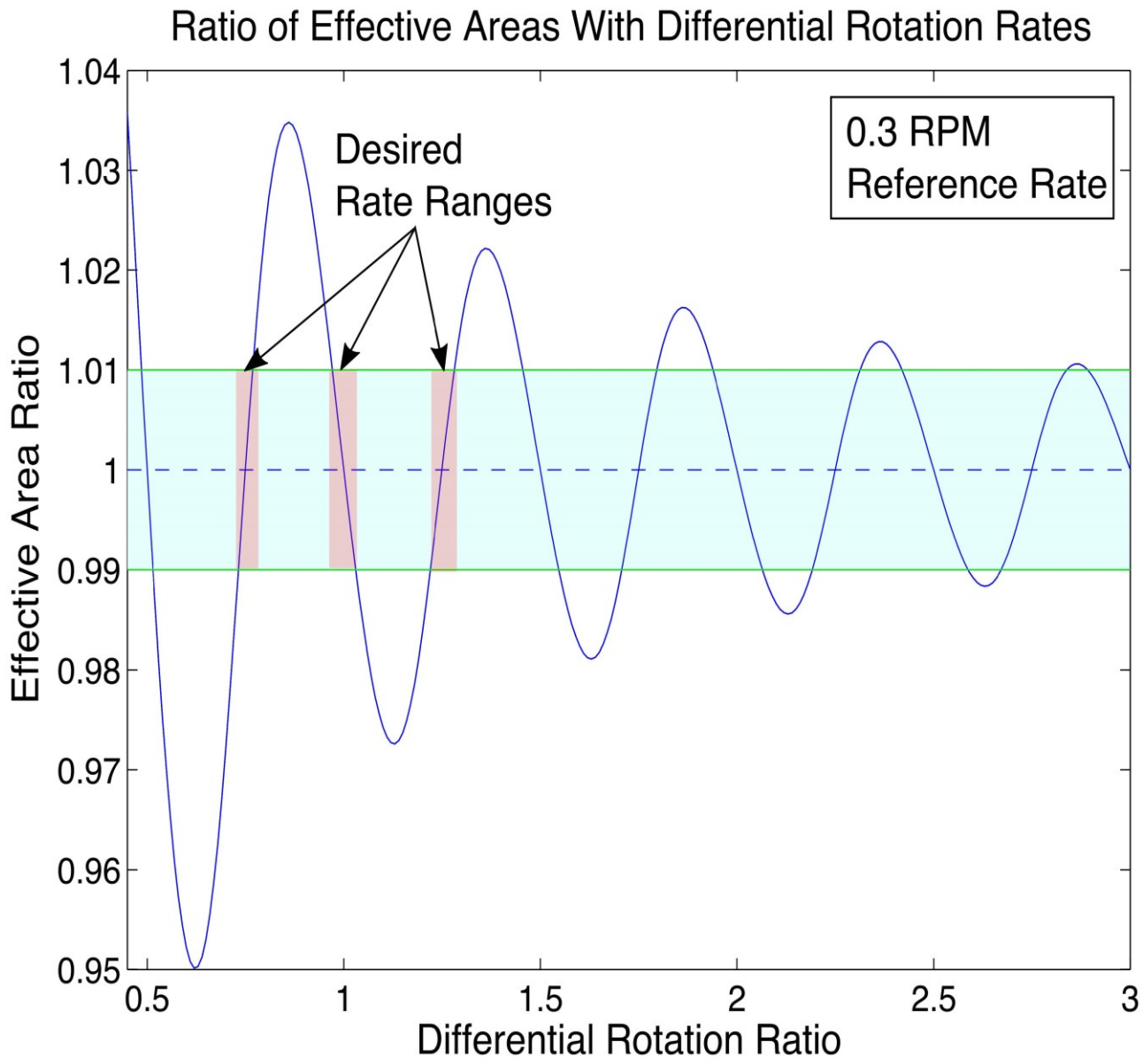

Figure 12. Ratio of effective drag areas for spacecraft rotation rates relative to the first spacecraft's rotation rate. The pink boxes show acceptable rotation rate ratios that do not impair the GPS receiver's ability acquire and maintain lock with a given GPS spacecraft.

opposite facing 100° FOV antennas orthogonal to the rotation axis. The spacecraft was propagated for one day in one-second increments, and access times to the GPS constellation were obtained. The access data was first filtered for elevation angles below the local horizon to select limb occulting geometries, and the spacing between the ray paths of each spacecraft was computed for each reported access azimuthal angle, ϕ. The spacing, ρ, represents the multipoint spatial resolution as defined in Figure 14. The ray path spacings were divided into fifty bins between 0–20 km of spacecraft separation. Figure 15 shows the results of this analysis as the percentage of time SCION achieves the desired spatial resolution with increasing spacecraft separation. The analysis was also performed for 40°, 55°, and 60° inclinations, and right ascension of the ascending node (RAAN) offsets of 0°, 15°, and 30°. This revealed that the RAAN offset

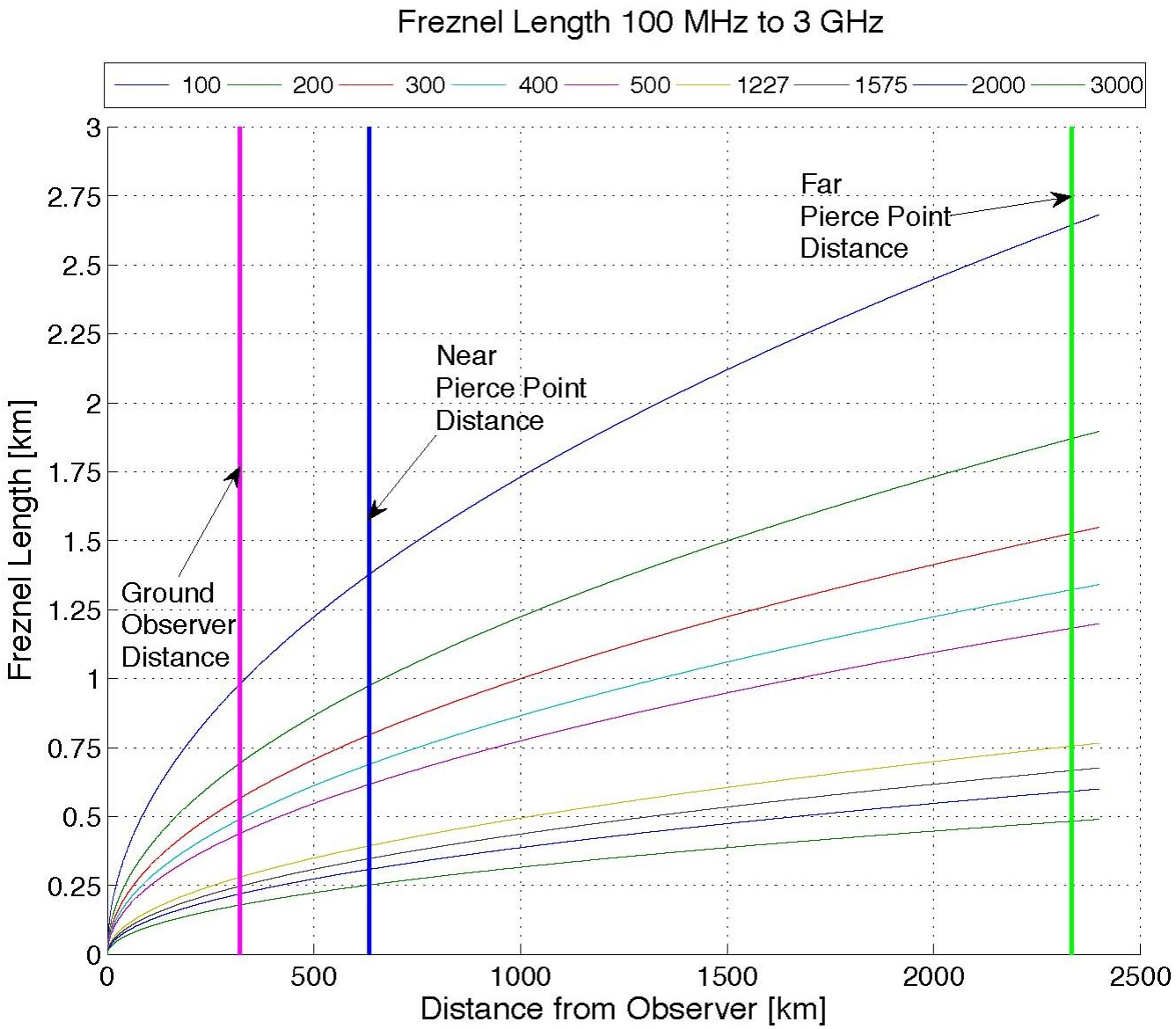

Figure 13. The range of Freznel length spatial scales observed by SCION and from the ground over a range of typical communication and navigation frequencies. The observation distance from the two F region pierce points, 600-2500 km, is much greater than that of a typical ground observer, 300 km. Accordingly, SCION does not experience scintillation while observing density structures that produce radio scintillation on the ground.

of the orbital plane relative to the principle GPS orbital planes was a significant factor. In fact, it demonstrated that the most frequent opportunities for observation at the desired scale occurred when SCION was in phase (the same RAAN) as one of the GPS orbital planes. This suggests that mission performance is affected by the launch's time of day. Comparing inclinations with equal RAAN, the greatest number of observation opportunities occurred when matching the GPS constellation's 55° inclination. Most importantly, this analysis shows that 1 km resolution is attainable for 20% of observations when the spacecraft are separated by 5 km, and up to 12% when the separation is 20 km. This fits well within the predicted spacecraft separation rate for 90 days.

Given the constraints on lifetime, the maximum possible altitude for SCION is 600 km. In order to achieve the minimum lifetime, its altitude must be

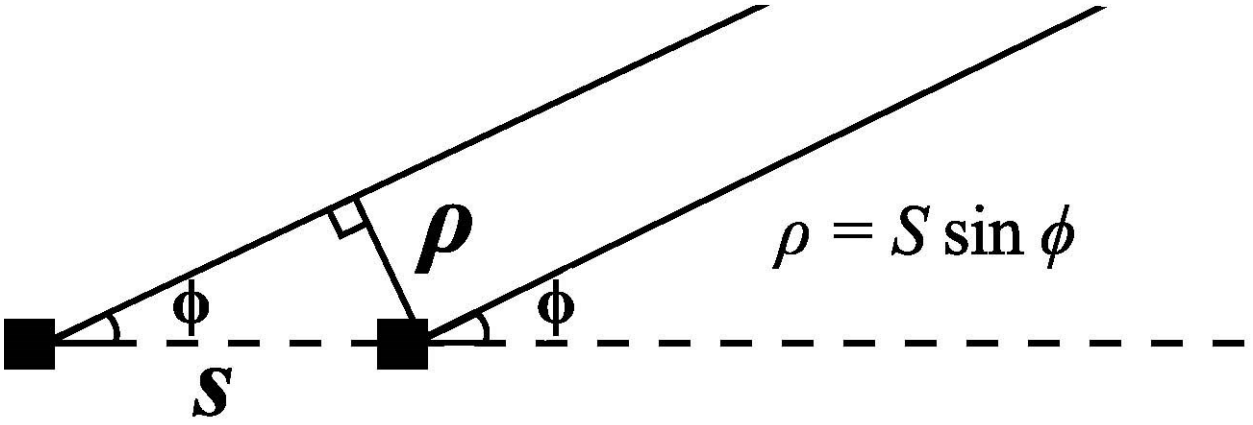

Figure 14. Schematic of the definition of multipoint spatial resolution, ρ, for varying spacecraft separation distances, S, given the azimuth angle, ϕ, in the local vertical, local horizontal reference frame.

above 450 km. For orbits below 700 km, inclinations between 40° and 60° provide the greatest average daily access time to both the GPS constellation and the Ann Arbor ground station. Finally, higher orbits and alignment with the one of the GPS orbital planes (55°, 0° offset from GPS RAAN) provided longer durations with observations at the desired spatial scales. A trade study based on these metrics concluded that while orbits of 40°–60° and 450–600 km are within the acceptable range, higher altitudes are preferred first, and then higher inclinations up to 60°. The ideal orbit for SCION is 600 km, 55° inclination, and with the RAAN initially aligned with the GPS constellation, suggesting a preference for the launch time of day.

3.4. Subsystem Overview

3.4.1. Spacecraft Structure

Each SCION spacecraft is built as a 1U (10 × 10 × 10 cm) structure, designed as a lightweight skeletonized aluminum structure similar to that used for CADRE and MCubed-2, allowing for easy insertion and removal of individual component modules and circuit boards. The structure will be made from Al 7075 aluminum with a hard anodized surface finish, as required by the CubeSat Design Specification, Rev. 13 (Pignatelli and Mehrparvar, 2014). Figure 16 shows the packaging and placement of key components and circuit boards within the SCION structure. In this configuration, there are at least 3–4 mm gaps between components. Two deployable solar arrays will unfold from opposite faces of the structure, using spring-loaded hinges. The panels are fully deployed 135° from their initial stowed position. A dual-frequency GPS patch antenna will be placed on each of the +/−X faces of the spacecraft pointed along the solar panel hinge axes to provide a minimally obstructed view of the GPS constellation, as shown in Figure 17.

3.4.2. Power

The power system consists of two serial 3.6V, 2.9 A hr Lithium-ion secondary batteries for a spacecraft V-batt bus voltage of 7.2 V regulated to 3.3 and 5 V lines. Power will be generated using deployable and body-mounted solar cells. The solar cells will be SpectroLab XTJ cells with beginning-of-life efficiency of 29.5% and degradation to an expected end-of-life efficiency of 26.1%, based on the anticipated radiation environment for SCION's potential orbits. Lifecycle power generation was estimated using STK to determine the illumination and solar incidence angle for each cell, given the ranges of season, orbit, orientation, and rotation rates expected during the mission. The analysis shows that this power generation system is able to provide 9.15 W in sunlight, with deployed solar panels of sufficient margin to

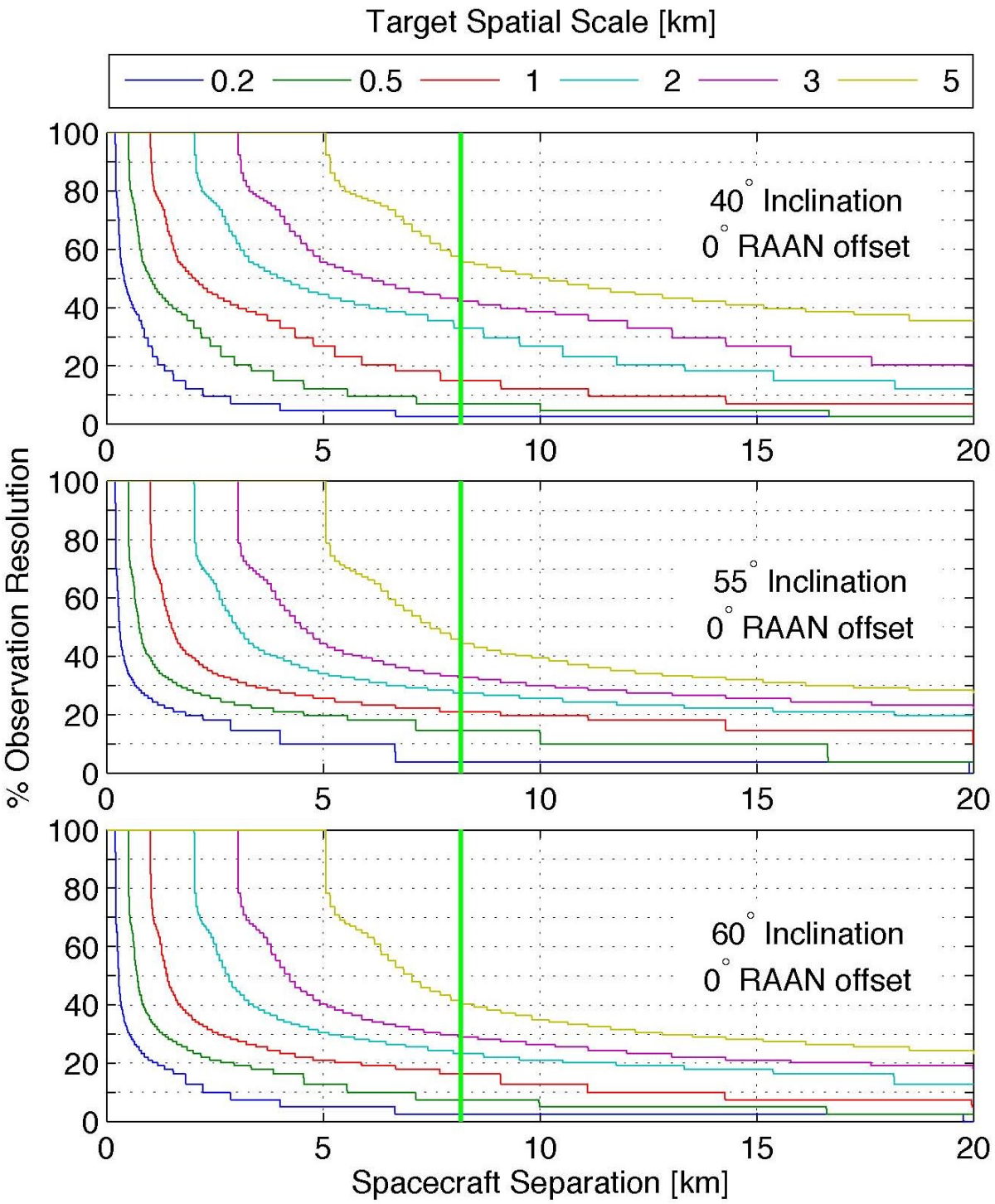

Figure 15. Percentage of observations within the target spatial resolution for spacecraft separations of 0–20 km. The orbital planes' RAAN are aligned with one of the GPS orbital planes (130°), and at inclinations of 40° (top), 55° (middle, matched to GPS inclination), and 60° (bottom). The vertical green line is the predicted separation distance at 90 days.

recharge batteries during the maximum power consumption of 3.06 W in the Science Operations Mode. Prior to solar panel deployment, the body-mounted solar panels produce 3.64 W, which is sufficient to fully recharge batteries in all modes except during detumbling. During detumbling, the batteries accu-

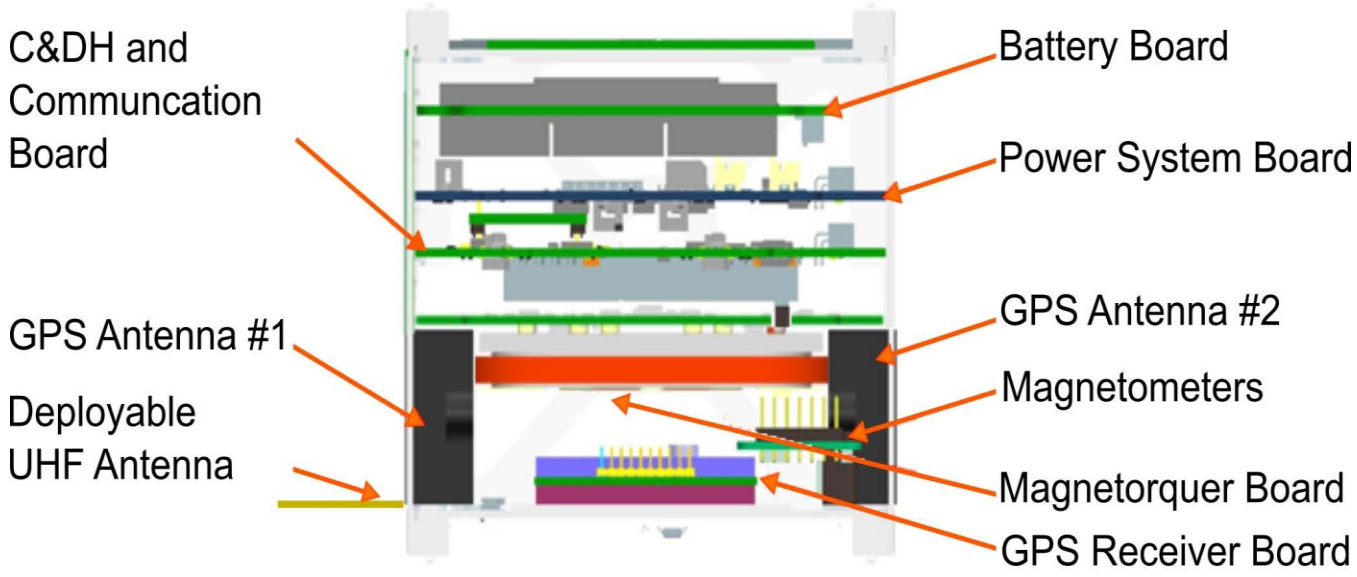

Figure 16. Cut-out showing packaging and placement of subsystem components within the SCION structure.

mulate a 5.5% depth-of-discharge (DOD) per orbit that is not replenished. Since detumbling is expected to be complete within two orbits, the batteries experience an 11% DOD for one cycle early in the mission. After solar panel deployment, the maximum operational (DOD) occurs during the longest predicted eclipse, which is 8.6% in the Science Operations Mode.

3.4.3. Command and Data Handling (CDH)

SCION's CDH board is a custom design based on similar CDH boards developed for the CADRE and FTS missions (Wloszek et al., 2013), and is heavily based on experience and flight heritage gained from the M-Cubed, RAX-1, and RAX-2 missions. The motherboard runs an embedded Linux kernel, and its core is a STAMP9G20 computer module containing an Atmel ARM9 processor. The CDH board's software will manage data collection, mode changes, and spacecraft functions, including communication protocols.

SCION's CDH subsystem responsibilities are listed in Table 2.

Table 1. Summary of Power Resources During each Mission Mode: Power, Margin, and Battery Depth of Discharge (DOD)

	Mission Modes				
	Safe	Detumble	Deploy	Standby	Sci Ops
Power [W]	0.81	1.96	0.83	1.48	3.06
Margin [W Hr][1]	2.43	0.58	2.40	7.01	4.47
DOD	2.3%	5.5%[2]	2.3%	4.2%	8.6%

[1]Margin refers to the energy available for battery charging

[2]During detumbling, the batteries accumulate a 5.5%DOD per orbit prior to solar panel deployment

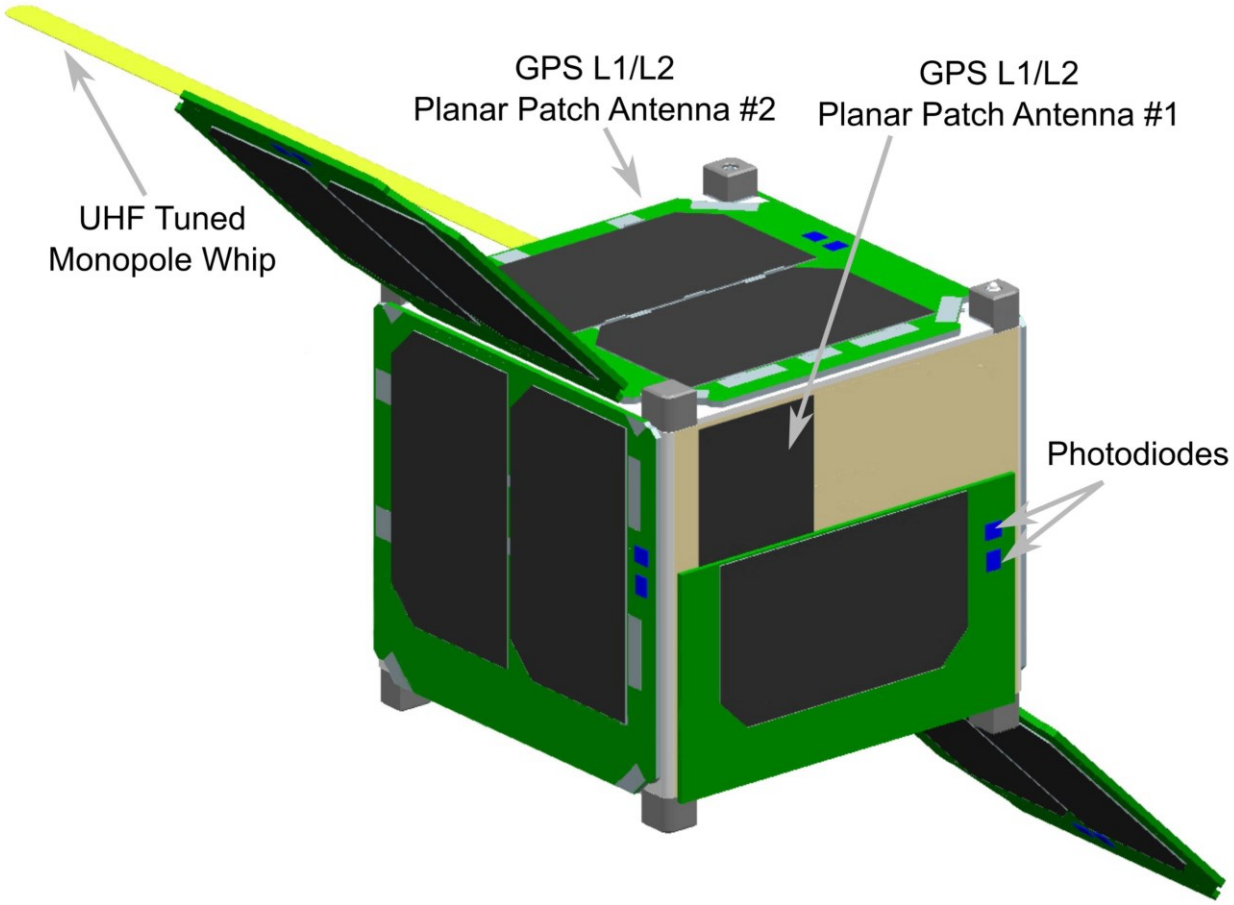

Figure 17. SCION with fully deployed panels at 135°, deployed UHF monopole antenna, and relative placement of GPS patch antennas.

The flight software runs on the STAMP9G20's SDRAM flash storage, which is partitioned to mitigate single event effects. If one kernel is corrupted, secondary or tertiary copies are used. After flashing all kernels for flight, the software team ensures that the kernels have the same CRC32 checksum. Thereafter, the CRC32 checksum is stored in the bootloader's (U-Boot) environment (env1, env2). Linux is unable to write to the kernel partitions, so any CRC32 error is due to a flash error, such as a bit flip. If anomalous behavior is suspected during flight, a reboot command is initiated from the ground. On boot,

Table 2. CDH Subsystem Responsibilities

Data Collection	Collection of data from the attitude determination sensors, the GPS science payload, and health and status sensors
Timekeeping	Onboard clock and command synchronization
Data Management	Storing, filtering, and compressing data for downlink
Attitude Control	Gathering attitude sensor information and running the attitude control algorithm
Comm. Management	Assembling health beacon and downlink packets; interpreting and executing ground station commands

if the first kernel does not match, U-Boot selects the second, if not that, it selects the third. If the third does not match either, U-Boot tries to boot from third regardless. It is possible for the U-Boot process to become corrupted, since it resides on the same NAND chips as the kernels. However, there are two U-Boot environment partitions that are selected though the NAND chips' native error correction code, which provides some redundancy against U-Boot corruption. SCION also uses three SDRAM storage banks with a veto error correction scheme. If one of the banks does not match the checksum of the other two, it is assumed the data on that bank has been corrupted, and data from the other two are used for the next downlink. The corrupted bank is then overwritten.

3.4.4. Communication

Each SCION spacecraft communicates directly with a single, dedicated UHF ground station at 42.29° N, −83.71° E, in Ann Arbor, Michigan. This ground station has been used successfully for previous CubeSat missions. It is half-duplex, meaning it can either transmit or receive, and can do so with any number of spacecraft, provided their communication channels do not overlap, they fit within the 432–440 MHz band, and are not separated by more than 15° in the ground station's field of view (~160 km separation at 600 km altitude). The data downlink is initiated and commanded from the ground. Science data is combined with basic housekeeping data consisting of currents, voltages, and temperatures (IVT) on the various subsystems, and onboard data compression is implemented to reduce the size of the downlinked data package.

Once data are received from SCION at the ground station, it is compiled into the Receiver Independent Exchange (RINEX) 2.11 geodetic data format. RINEX is not a compact format, and therefore producing and transmitting a complete RINEX file from SCION file is prohibitive. Fortunately, much of the data required to create a RINEX file (for example, GPS ephemerides) are available on the ground and do not require information from the receiver itself. Consequently, SCION will only downlink the minimum observables required to reconstruct a RINEX file on the ground. Even still, the large data volume generated by the GPS receiver presents one of the greatest challenges of the SCION mission design. Analysis of access to the GPS constellation from a single SCION spacecraft shows that the maximum number of GPS spacecraft in view at any given point of the SCION mission is ten. Sampling all ten GPS satellites at a peak rate of 50 Hz produces 1.2 GB of data per day, whereas at 1 Hz, the data volume drops to 26.8 MB per day. Onboard 1:4 data compression using tar+bzip2 reduces this volume, but the high sample rate data volume still exceeds the present capabilities of most CubeSat radios. Assuming a circular orbit at 600 km altitude, 40° inclination, SCION will make on average six ground station contacts per day, each 11 min in duration, over the course of a year. Based on these assumptions, Table 3 summarizes the data volume and downlink rate required for three sample rates.

Table 3. Required Downlink Rate for Zero Backlog Given GPS Sample Rate, Including Housekeeping Data, Assuming 1:4 Compression

Sample Rate	Per day	Required Rate
5 Hz	125 MB	75.2 kbps
20 Hz	493 MB	296.5 kbps
50 Hz	1,230 MB	739.3 kbps

Communication link analysis found that a UHF downlink is insufficient to transmit all data generated at the desired 50 Hz cadence. However at a sample rate of 5 Hz, the returned data volume is feasible using an AstroDev Lithium UHF radio capable of transmitting at 76,800 bps and closing the link with 3.65 dB margin using a single UHF-tuned monopole antenna.

Fortunately, it is not necessary to transmit data from all measurement geometries at the same rate. For instance, data from GPS satellites that fall within the field of view of the side-scanning geometry should be included in the downlink at as high a rate as possible, whereas data from the limb occultation geometry can be much lower at 0.1 Hz. The advantage of this approach is that the receiver can sample all geometries at its peak rate, but onboard filter-

ing algorithms can determine at which rate different observations are added to the downlinked data package. To quantify this, an effective data rate was calculated as the weighted average of the sample rates for each of the three measurement geometries and STK was used to determine the typical number of GPS satellites in the FOV of those geometries over a one-month epoch (Figure 6).

Table 3 demonstrates that the effective sample rate must be below 5 Hz to achieve the requirement of zero data backlog over the mission lifetime. In actuality, the true rate is closer to 4.6 Hz, to allow a 10% downlink rate margin. Table 4 shows an example scenario that uses this technique to achieve a 5 Hz effective sample rate while reporting high rate data when it is useful.

Table 4. Typical Number of Satellites in Each Measurement Geometry at any Given Time, with Respective Sample Rates and Spatial Resolution

	Returned Rate	# GPS in View	Spatial Resolution
Topside	20 Hz	0.2	0.35 km
Sidescan	35.7 Hz	1.2	0.20 km
Limb	0.1 Hz	0.3	1.50 km

3.4.5. Attitude Determination and Control (ADCS)

SCION does not have strict pointing requirements, since the GPS and communication antennas can function in almost any orientation. However, it does require a controlled rotation rate. Therefore, the design drivers for the ADCS system are to detumble after PPOD deployment, and to control spacecraft rotation. Controlled rotation is crucial to SCION, and accomplishes two things. First, it sweeps the GPS antennas slow enough to acquire a fix on both frequencies and make observations. Second, it supports the passive spacecraft separation concept described in Section 3.3.4. To accomplish this, SCION is equipped with a magnetorquer board similar to that shown in Figure 18 containing an air core magnetorquer and two solid-core magnetic torque rods. Small magnetometers and photo-diodes will provide sufficient attitude knowledge of coarse alignment relative to the local magnetic field and rotation rate, respectively. The solar cells will also provide additional coarse attitude information.

The ADCS concept of operations uses the magnetorquers after deployment to detumble the spacecraft to a coarse alignment of the +Z axis with the Earth's magnetic field. It is expected that it will take approximately two orbits to achieve magnetic alignment. Once detumbling is accomplished, the magnetorquer board will achieve an initial +Z alignment with the Earth's magnetic field at the equator (northward). The magnetorquer board will then be put into a standby state that only actuates as necessary to maintain the northward +Z alignment. A software control loop running on a dedicated FPGA will drive the magnetic torque rods to achieve the desired rotation rate about the spacecraft +Z axis. To produce this rotation, the magnetic torque rods will actuate when the +Z axis is oblique to the magnetic field, which occurs at higher magnetic latitudes. For example, at 40° geomagnetic latitude, the magnetic inclination, or dip angle, is 55–68°, depending on longitude. Since the spacecraft orientation is aligned with the equatorial magnetic field, as it nears high latitudes, the magnetic field is 90–108° relative to the spacecraft +Z axis. The magnetic torque rods along the X and Y axes are properly aligned to produce rotation about the +Z axis. The FPGA controller actuates the magnetic torque rods to spin the spacecraft to a baseline spin rate of ~0.3 RPM, though the spin rate can be updated during the mission.

ADCS sizing considered disturbance torques from aerodynamic, solar pressure, residual spacecraft magnetic dipole, and gravity gradient forces with the following assumptions: The worst-case aerodynamic and solar pressure centers of pressure were assumed to be centered on one of the deployed solar panels with a moment arm of 12.1 cm. The worst-case residual dipole was assumed from Springmann et al., 2010 as 0.01 A m^2 and Earth's magnetic field at was taken as 45,294 nT from the International Geomagnetic Reference Field (IGRF), which is the maximum for 60° geodetic latitude and 500 km altitude. Last, the worst case gravity gradient was calculated from the maximum difference in mass moment of inertias

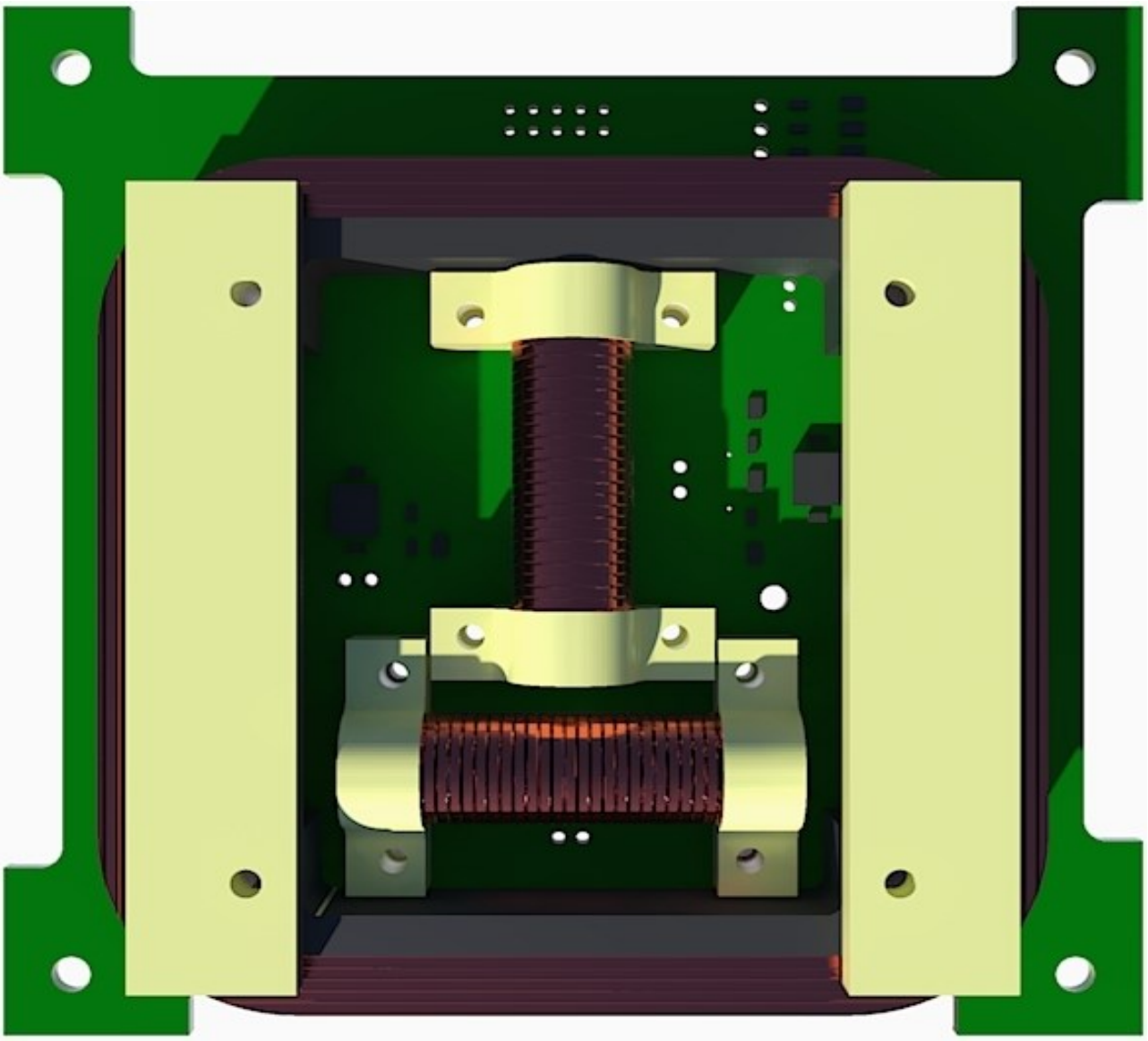

Figure 18. Rendering of a PCB mounted air core magnetorquer (outer winding) and two solid core magnetic torque rods flown on the GRIFEX mission. A similar system will be used on SCION. Image credit: Michigan eXploration Laboratory (MXL).

along the spacecraft principle axes. The disturbance torques are summarized in Table 5.

The magnetic torque rods aligned with the spacecraft X and Y axes need a magnetic moment of 0.015 A m^2 to produce the required torque for maximum disturbance rejection in the weakest magnetic field, near the magnetic equator. Sizing the magnetic actuators at the weakest geomagnetic field for the greatest magnetic disturbance torque at the strongest geomagnetic field provides an inherent safety factor of 1.5 due to the relative strengths of Earth's magnetic field

Table 5. Summary of Worst-case Disturbance Torques at 500 km and 60° (The worst-case residual magnetic torque is assumed from Springmann et al. (2010).)

Disturbance	Torque [N m]
Aerodynamic	1.38E-07
Solar Pressure	1.56E-08
Residual Magnetic	*4.53E-07*
Gravity Gradient	1.18E-09
Safety Factor (SF)	3.0
Maximum Disturbance	1.36E-06

at these points in the orbit. Furthermore, to spin the spacecraft at high-latitude magnetic inclinations, an additional 0.02 A m^2 is required to spin up the spacecraft in the 100 s it takes to travel northward between 35° and 40° latitude. The variation in magnetic inclination over this period is between 64.5° and 68°. The in-house PCB embedded magnetorquer board has a calculated magnetic dipole moment of ~0.055 A m^2 in all three axes, which provides a net safety factor of 3.0 over the worst case disturbance torque to ensure magnetic alignment. Commercially available CubeSat magnetic torque rods with a magnetically soft core (ferrite, Metglas®, nickel alloy, etc.) can also reasonably produce a magnetic moment of 0.1 A m^2, providing a net safety factor of 4.5.

4. Conclusion and Future Work

SCION represents a concept for a rapidly developed, low-cost, and focused scientific mission to answer important questions about the nature of mid-latitude scintillation and the small-scale density structure in the ionosphere. An important result of this study is the overall feasibly of such a mission from the CubeSat platform. Much of the future work for SCION centers on developing the necessary control algorithms for the spacecraft spin rate, further modeling of aerodynamic drag forces and spacecraft separation, and improved methods to downlink the large data volume produced. Fortunately, the remaining technical challenges have credible solution paths that will help to fully realize this mission with continued work.

Acknowledgments

Funding for this research was provided by the National Science Foundation under awards ASG 1265651, AGS 1111476, and AGS 1342968 and by the National Aeronautics and Space Administration under award NNX14AF31G.

The authors thank the reviewers and the following for their suggestions, assistance, and support: Aaron Ridley, James Cutler, Doug Sinclair, Arie Sheinker, Theresa Carranza, Adam Werries, Srinagesh Sharma, Kathryn Luczek, Ari Porter, Josh Weiss, and Catherine Houlahan.

References

Anthes, R. A. et al. (2008): The COSMIC/FORMOSAT-3 Mission: Early Results, *Bulletin of the American Meteorological Society*, vol. 89(3), pp. 313–333.

Arlas, J. and Spangelo, S. (2013): GPS Results for the Radio Aurora Explorer II CubeSat Mission, in *Proceedings of the AIAA Region III Student Conference*, Ann Arbor, MI: American Institute of Aeronautics and Astronautics.

Basu, S. and Groves, K. M. (2001): Specification and Forecasting of Outages on Satellite Communication and Navigation Systems, in P. Song, H. J. Singer, and G. L. Siscoe (eds.), *Space Weather*, pp. 423–430, American Geophysical Union.

Brahmanandam, P. S. et al. (2012): Global S4 Index Variations Observed Using FORMOSAT-3/COSMIC GPS RO Technique During a Solar Minimum Year, *Journal of Geophysical Research: Space Physics*, vol. 117(A9), p. A09,322.

Chen, F. F. (1984): *Introduction to Plasma Physics and Controlled Fusion*, 2nd ed., New York: Plenum Press.

Crowley, G. et al. (2011): Dynamic Ionosphere Cubesat Experiment (DICE), in *Proceedings of the 25th Annual AIAA/USU Conference on Small Satellites*.

Dalgarno, A. and Smith, F. J. (1962): The Thermal Conductivity and Viscosity of Atomic Oxygen, *Planetary and Space Science*, vol. 9(1–2), pp. 1–2.

Damasceno Ferreira, L. D. and Jaime Da Cruz, J. (1991): Attitude and Spin Rate Control of a Spinning Satellite Using Geomagnetic Feld, *Journal of Guidance, Control, and Dynamics*, vol. 14(1), pp. 216–218.

Datta-Barua, S. et al. (2003): Ionospheric Scintillation Effects on Single and Dual Frequency GPS Positioning, in *Proceedings of ION GPS/GNSS*, pp. 336–346.

Dyrud, L. and Fentzke, J. T. (2011): GEOScan Planning Workshop Report, in *Proceedings from the GEOScan Planning Workshop*, Annapolis, MD.

Fong, C. J. et al. (2007): GPS Radio Occultation and Mission Results from FORMOSAT-3/COSMIC Spacecraft Constellation, in *Recent Advances in Space Technologies, 2007. RAST'07. 3rd International Conference on*, pp. 748–753, IEEE.

Foster, J. C. (2005): Midlatitude TEC Enhancements During the October 2003 Superstorm, *Geophysical Research Letters*, vol. 32(12).

Hajj, G. A. and Romans, L. J. (1998): Ionospheric Electron Density Profiles Obtained with the Global Positioning System: Results from the GPS/MET Experiment, *Radio Science*, vol. 33(1), pp. 175–190.

Hinch, E. J. (1988): Hydrodynamics at Low Reynolds Numbers: a Brief and Elementary Introduction, in *Disorder and Mixing*, pp. 43–56, Springer.

Ledvina, B. M., Makela, J. J., and Kintner, P. M. (2002): First Observations of Intense GPS L1 Amplitude Scintillations at Midlatitude, *Geophysical Research Letters*, vol. 29(14), p. 1659.

Mannucci, A. J., Wilson, B. D., and Edwards, C. D. (1993): A New Method for Monitoring the Earth's Ionospheric Total Electron Content Using the GPS Global Network, Technical Report, Jet Propulsion Laboratory.

NASA-STD-8719.14A (2012): Process for Limiting Orbital Debris.

NPR 8715.6A (2009): NASA Procedural Requirements for Limiting Orbital Debris, Technical Report, National Aeronautics and Space Administration.

Pi, X. et al. (1997): Monitoring of Global Ionospheric Irregularities using the Worldwide GPS Network, *Geophysical Research Letters*, vol. 24(18), pp. 2283–2286.

Pignatelli, D. and Mehrparvar, A. (2014): CubeSat Design Specification Rev 13.

Prikryl, P. et al. (2010): GPS TEC, Scintillation and Cycle Slips Observed at High Latitudes During Solar Minimum, *Annales Geophysicae*, vol. 28(6), pp. 1307–1316.

Sabol, C., Burns, R., and McLaughlin, C. A. (2001): Satellite Formation Flying Design and Evolution, *Journal of Spacecraft and Rockets*, vol. 38(2), pp. 270–278.

Sorensen, J. A. (1971): A Magnetic Attitude Control System for an Axisymmetric Spinning Spacecraft, *Journal of Spacecraft and Rockets*, vol. 8(5), pp. 441–448.

Springmann, J. C., Cutler, J. W., and Bahcivan, H. (2010): Magnetic Sensor Calibration and Residual Dipole Characterization for Application to Nanosatellites. Toronto, American Institute of Aeronautics and Astronautics.

Sun, Y. Y. et al. (2013): Ground-based GPS Observation of SED-associated Irregularities over CONUS: SED-associated Irregularities over CONUS, *Journal of Geophysical Research: Space Physics*, vol. 118(5), pp. 2478–2489.

Tsybulya, K. and Jakowski, N. (2005): Medium and Small-scale Ionospheric Irregularities Detected by GPS Radio Occultation Method, *Geophysical Research Letters,* vol. 32(9).

Vallado, D. A. and Finkleman, D. (2008): A critical assessment of satellite drag and atmospheric density modeling, in *AIAA/AAS Astrodynamics Specialist Conference and Exhibit*, pp. 18–21.

Van Dierendonck, A., Klobuchar, J., and Hua, Q. (1993): Ionospheric Scintillation Monitoring Using Commercial Single Frequency C/A Code Receivers, in *Proceedings of the 6th International Technical Meeting of the Satellite Division of The Institute of Navigation (ION GPS 1993)*, pp. 1333–1342, Salt Lake City, UT.

Wloszek, P. et al. (2013): FTS CubeSat Constellation Providing 3D Winds.pdf, in *Proceedings of the 27th Annual AIAA/USU Conference on Small Satellites*, Logan, UT.

Yizengaw, E. et al. (2012): Longitudinal Differences of Ionospheric Vertical Density Distribution and Equatorial Electrodynamics, *Journal of Geophysical Research (Space Physics)*, vol. 117, pp. 1–10.

Yizengaw, E. et al. (2008): The Occurrence of Ionospheric Signatures of Plasmaspheric Plumes over Different Longitudinal Sectors, *Journal of Geophysical Research*, vol. 113(A8), pp. 1–9.

Yizengaw, E. et al. (2006): First Tomographic Image of Ionospheric Outflows, *Geophysical Research Letters*, vol. 33(20), pp. 1–5.

Yizengaw, E. et al. (2005): Southern Hemisphere Ionosphere and Plasmasphere Response to the Interplanetary Shock Event of 29–31 October 2003, *Journal of Geophysical Research: Space Physics*, vol. 110(A9), pp. 1–16.

Zou, S. et al. (2014): On the Generation/Decay of the Storm-Enhanced Density (SED) Plumes: Role of the Convection Flow and Field-Aligned Ion Flow, *Journal of Geophysical Research: Space Physics*, p. 2014JA020408.

Zou, S. et al. (2013): Multi-instrument Observations of SED During 24-25 October 2011 Storm: Implications for SED Formation Processes, *Journal of Geophysical Research (Space Physics)*, vol. 118, pp. 7798–7809.